1-1-2005

Estimation and equalization strategies for fiber-wireless communications in a multiuser CDMA environment

Stephen Z. Pinter
Ryerson University

ESTIMATION AND EQUALIZATION STRATEGIES FOR FIBER-WIRELESS COMMUNICATIONS IN A MULTIUSER CDMA ENVIRONMENT

by

Stephen Z. Pinter
B.Eng. (Hons.), Ryerson University, Canada, 2003

A thesis
presented to Ryerson University
in partial fulfillment of the
requirement for the degree of
Master of Applied Science
in the Program of
Electrical and Computer Engineering.

Toronto, Ontario, Canada, 2005

Author's Declaration

I hereby declare that I am the sole author of this thesis.

I authorize Ryerson University to lend this thesis to other institutions or individuals for the purpose of scholarly research.

Author's Signature

I further authorize Ryerson University to reproduce this thesis by photocopying or by other means, in total or in part, at the request of other institutions or individuals for the purpose of scholarly research.

Author's Signature

Instructions for Borrowers

Ryerson University requires the signatures of all persons using or photocopying this thesis. Please sign below, and give address and date.

Name	Signature	Address	Date

Abstract

Estimation and Equalization Strategies for Fiber-Wireless Communications in a Multiuser CDMA Environment

Master of Applied Science
Department of Electrical and Computer Engineering
Ryerson University

Two major issues associated with fiber-wireless technology are the nonlinear distortion of the optical link and the multipath dispersion of the wireless channel. In order to limit the effects of these distortions, estimation, and subsequently equalization of the concatenated fiber-wireless channel needs to be done. This thesis addresses three scenarios in this regard, they are: uplink estimation using pseudonoise (PN) sequences, downlink estimation using Walsh codes, and uplink equalization using a decision feedback equalizer (DFE) and series reversion, all in the presence of both wireless and optical channel noise. The training sequences used in the identification are practically feasible. These training sequences have white noise-like properties which effectively decouples the identification of the linear and nonlinear channels. Correlation analysis is then applied to identify both systems. Furthermore, we propose an algorithm to mitigate the adverse effect of multiple access interference (MAI). Numerical evaluations show a good estimation of both the linear and nonlinear systems with 10 users for the uplink and 54 users for the downlink, both with a signal-to-noise ratio (SNR) of 25 dB. Chip error rate (CER) simulations show that the proposed MAI mitigation algorithm leaves only small residual MAI.

Acknowledgements

First and foremost, a special thanks to my supervisor Dr. Xavier Fernando for his expertise, approachability, and continued support throughout this entire process. I would also like to thank the members of ADROIT for helpful discussions and feedback during our research group meetings.

I would like to acknowledge the financial support provided by the Ontario Graduate Scholarship (OGS), the research funding of my supervisor allowing for a stipend, and Ryerson University for a graduate scholarship and academic assistantships. These funding sources helped make this work possible and are much appreciated.

I wish to express my deepest thanks to my family for their help and support throughout this process. To my parents for providing me with this opportunity, and to my sister for encouragement and advice along the way. This work is a reflection of their commitment as well and I am truly grateful.

Contents

List of Figures

List of Tables

List of Abbreviations and Acronyms

ARMA	auto regressive moving average
APD	avalanche photodiode
CDMA	code division multiple access
CER	chip error rate
CIR	channel impulse response
CMT	cross multiplied terms
DFE	decision feedback equalizer
DSSS	direct sequence spread spectrum
FBF	feedback filter
FFF	feed forward filter
FHSS	frequency hopping spread spectrum
ISI	intersymbol interference
LFSR	linear feedback shift register
LHS	left hand side
LTI	linear time invariant
MAI	multiple access interference
MISO	multiple input single output
MSE	mean square error
MU	multiuser with a different wireless channel for each user
MUc	multiuser with a common wireless channel for each user
OWNN	orthogonal wavelet-based neural network
PN	pseudonoise
PRBS	pseudo-random bit sequence
RAP	radio access point
RF	radio frequency
RHS	right hand side
RIN	relative intensity noise
RLS	recursive least squares
ROF	radio-over-fiber
SNR	signal-to-noise ratio
SVD	singular value decomposition
THSS	time hopping spread spectrum

Chapter 1

Introduction

1.1 Overview of fiber-wireless technology

Wireless technology is a major part of everyday communications. From cell phones to E-commerce to personal computers, wireless communications is widespread in both indoor and outdoor environments. Wireless technologies have emerged from simply transmitting voice, to multimedia services such as videos, pictures, and data. Present consumers are not interested in the underlying technology; they simply need reliable and cost effective communication systems that can support *anytime, anywhere, any media* they want. Furthermore, new wireless subscribers are signing up at an increasing rate demanding more capacity while the radio spectrum is limited. As a result of these ever increasing demands comes the need for broadband access. One of the technologies proposed to satisfy this increasing demand suggests integration of the high capacity of optical networks with the flexibility of radio networks; this is referred to as radio-over-fiber (ROF), a fiber-based wireless access scheme ([1], [2], [3]). By combining these two areas, ROF strives to meet the demand for growing broadband access.

1.1.1 Cell architecture

The fiber-wireless architecture for cellular networks is shown in Figure 1.1. In this scenario there is an intermediate stage between the central base station and the mobile units. This intermediate stage is the optical fiber and the radio access point (RAP in Figure 1.1). The RAPs provide wireless access instead of the conventional base station, and are connected to

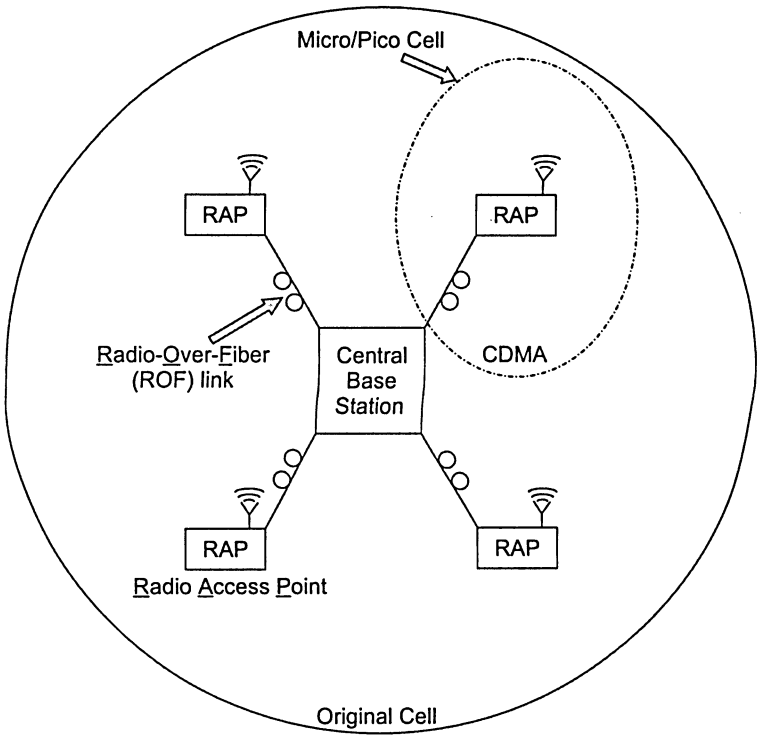

Figure 1.1: Fiber-wireless cellular architecture.

the central base station via the ROF links. In the downlink, the radio frequency (RF) signal is transmitted through the optical fiber, via subcarrier transmission, and is radiated to the mobile units upon being received at the RAP. The opposite takes place in the uplink. Using the RAPs as an intermediate base station allows for a mirco/pico cell scenario; the micro cell having a cell radii of 200 m to 1 km, and the pico cell having a cell radii of 10 m to 200 m. It is important to keep the RAPs complexity, cost, and power at a minimum in order to allow for large scale deployment. By doing so, a large cell can easily be split into smaller cells by dispersing RAPs throughout. This increases frequency reuse and enables broadband access.

Several observations can be made from Figure 1.1. First, signal processing should not be done at the RAP for cost considerations. Therefore, compensation should be done at the mobile unit or at the central base station. By performing most of the signal processing at the central base station, i.e. by asymmetric distribution of the complexity, the cost can be shared by many users and therefore helps reduce overall system cost. Second, the compensation

of the concatenated fiber-wireless channel should be handled jointly. This is a challenging task because of the time varying multipath wireless channel in series with the nonlinear optical channel. Furthermore, the uplink and downlink require different solutions. Third, it is desirable not to modify the portable units because of the ROF link. In other words, the portable unit should not be aware of the existence of the ROF link. This makes seamless roaming between fiber-based and conventional wireless systems possible.

1.1.2 Radio-over-fiber transmission

In order to get the RF signal from the base station to the RAP, or from the RAP to the base station, the RF signal must be transmitted along the optical fiber. This is done by modulating an optical signal at radio frequencies and then transmitting the optical signal through the optical fiber. This is referred to as analog subcarrier transmission, which is shown in Figure 1.2. Here, the RF signal rides along the RF modulated optical carrier. At the receiving end of the optical fiber, the RF signal is demodulated and transmitted to the corresponding wireless user.

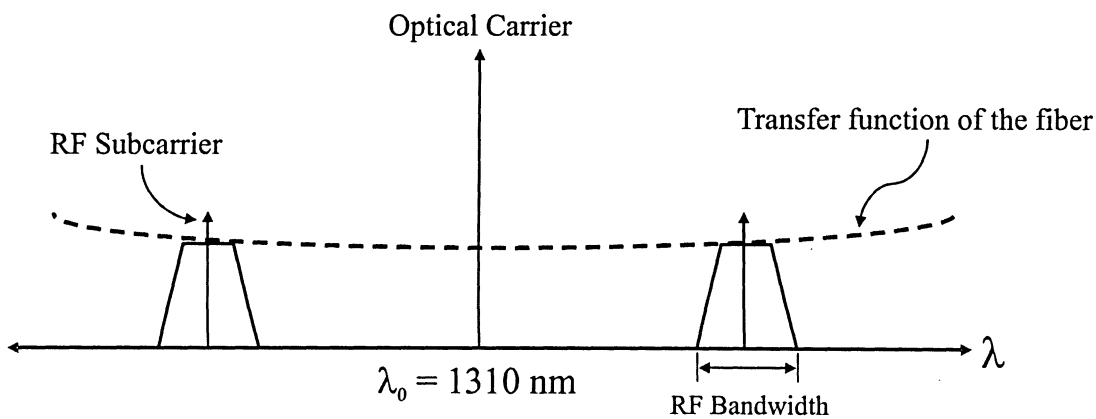

Figure 1.2: Spectrum of subcarrier transmission [4].

Subcarrier transmission allows ROF technology to alleviate the increasing demand for broadband services through the implementation of the previously discussed micro/pico cellular architectures. Advantages of ROF include:

- Large optical bandwidth enables the multiplexing of several radio channels,

- Multiple services can be transmitted on a single fiber; each radio channel may belong to a different system such as wireless LAN (IEEE 802.11) or cellular radio (CDMA),
- Line-of-sight operation minimizes the effect of multipath dispersion,
- Ability to use existing dark/dim fibers to transmit the radio signal (dim fiber can be used with WDM techniques),
- Inherent immunity to electromagnetic interference,
- Allowing for transparent operation and easy integration and upgrades; attributed to the fact that the RF to optical modulation is typically independent of baseband to RF modulation format,
- Enhanced cellular coverage in indoor environments such as offices, airport terminals, and shopping malls, and
- System coverage can be extended by simply connecting additional low cost, low power RAPs.

Conventional transmission mediums such as copper coaxial may not be completely replaced by optical fiber, but in applications where factors such as RF power loss, future system upgrades and transparency are considered, fiber is regarded as the most practical and efficient medium. Though the prospects of ROF are substantial, there is still plenty of research to be carried out in this area before widespread deployment can be considered.

1.2 Contributions

This thesis addresses some of the dominant issues associated with fiber-wireless transmission, these include: intersymbol interference (ISI), multiple access interference (MAI), nonlinearity, and performance evaluation in the presence of noise (these distortions will be elaborated upon in Section 2.2). ISI is a major concern because it is coupled with the nonlinear distortion of the optical link. In order to limit the effect of these distortions, estimation, and subsequently equalization of the concatenated fiber-wireless channel should be done. The

goal in this thesis is to first estimate the parameters of the fiber-wireless channel and then to devise appropriate equalization and compensation. The estimation is performed by applying correlation analysis, which is a control systems technique, to the area of wireless communications.

Equalization can be performed in one of two ways. Either the equalizer coefficients can be calculated based on estimates of the channel parameters, or adaptive techniques can be used to directly adjust the equalizer coefficients in order to minimize the error between the equalized signal and a training sequence. So why is one method preferred over the other and why is equalization via estimation employed in this thesis? Major drawbacks of adaptive techniques include increased complexity and even a single decision error in the recursive least squares (RLS) algorithm can disturb the adaptation process [5]. On the other hand, the estimation technique is found to be a potentially fast converging technique. It is a good candidate for equalization because non-adaptive adjustment of the equalizer coefficients makes the algorithm more robust in rapidly dynamic wireless channels [5]. However, the effectiveness depends on the quality of the channel impulse response (CIR) estimate. A major drawback with equalization via estimation is the overhead associated with the transmission of a training sequence. Typically, training is used to converge a filter at startup as part of the initialization overhead; then adaptation techniques can be used to track and compensate for minor variations in the CIR [6]. Perhaps this combination of both techniques is most suitable.

The work in this thesis stems from two major pieces of literature. The first is [7], where the authors' perform a complete identification of the fiber-wireless uplink using a single pseudonoise (PN) sequence and in the presence of a single noise term. The second is [8] (and the references therein), where the authors' analyzed the Wiener model (fiber-wireless uplink) under the excitation of a single PN sequence in a continuous-time baseband environment. A more practical application calls for extending identification to a multiuser environment, as well as including the effects of both wireless and optical channel noise. The major contributions of this thesis are summarized below:

1. The channel parameters of the fiber-wireless uplink are estimated in a multiuser CDMA

environment using **PN sequences**. The CIR of each user is estimated along with the nonlinearity of the common optical link.

- Wiener system estimation theory is derived for a multiuser discrete-time passband system.
- Since MAI is a major concern in a multiuser environment, an algorithm is developed to mitigate this issue and is shown to significantly improve the estimation in the presence of multiple users.

2. Estimation of the *wireless channel* of the fiber-wireless downlink in a multiuser CDMA environment is done using multiple **Walsh codes**.
   - Hammerstein system estimation theory is derived for a multiuser discrete-time passband system.
3. The fiber-wireless uplink is equalized in a single user environment while using the estimated channel parameters from the multiuser case. A decision feedback equalizer (DFE) is used to equalize the wireless channel and series reversion is used to compensate for the nonlinearity.
4. The effects of both wireless and optical channel noise are studied by error rate analysis.

The use of PN sequences for estimation of the fiber-wireless uplink, and Walsh codes for estimation of the fiber-wireless downlink, is attractive because these spreading codes are already widely used in spread spectrum communications [1]. They are practically feasible training sequences. To the author's knowledge, there is no work reported so far that looks specifically at identifying the multiuser fiber-wireless uplink using PN sequences, as well as identifying the multiuser fiber-wireless downlink using Walsh codes.

Although the work in this thesis is tailored to a multiuser fiber-wireless CDMA communication system, it can also be applied to areas outside of the communication field where a parallel connection of multiple linear systems is encountered in series with a single nonlinearity.

1.3 Organization

The rest of this thesis is organized as follows. Chapter 2 introduces some more background material (in addition to that of Chapter 1) on fiber-wireless communication using ROF technology. Issues such as ISI, MAI, noise, and nonlinearities are discussed in detail. It is essential to thoroughly review ROF because it is still relatively new. An overview of nonlinear systems theory is then presented, specifically looking at its application to the fiber-wireless channel. To end the chapter, direct sequence spread spectrum communications is discussed where the focus is mainly on describing spreading codes, i.e. PN and Walsh, and their properties.

Chapter 3 highlights related literature on Wiener and Hammerstein (block-oriented) system identification. An overview of different identification algorithms is covered, along with some discussion pertaining to the multiuser aspect of identification.

Chapter 4 applies correlation analysis to estimate the fiber-wireless uplink using PN sequences. A small section on baseband and passband representation precedes this discussion. Three different fiber-wireless scenarios are covered, with the MU case being the most important. A complete analytical treatment on using correlation analysis to estimate the wireless and optical channels in a multiuser environment is given. In addition, an iterative algorithm to remove MAI is proposed. The chapter concludes with a discussion of the simulation results.

Equalization of the fiber-wireless uplink is covered in Chapter 5; the wireless channel by DFE and the nonlinear channel by series reversion. Some related work on nonlinear compensation is presented and the advantages and disadvantages of series reversion are given. Simulation results are discussed next by obtaining an error rate analysis, i.e. chip error rate (CER). Several conclusions regarding the chosen estimation and equalization algorithms are drawn from the CER.

Chapter 6 applies correlation analysis to estimate the fiber-wireless downlink using Walsh codes. The derivation of key correlation relationships is shown. A difficulty with using Walsh codes is presented, as well as a discussion on how to overcome it. The chapter concludes with

simulation results on wireless channel estimation. Equalization of the downlink is performed using a DFE, and CER results are discussed.

Conclusions of the thesis are given in Chapter 7. The major contributions are summarized, and possible directions for future research are suggested. Lastly, appendix A contains a discussion on the multinomial theorem.

Chapter 2

Background

2.1 Fiber-wireless system model

An overview of the fiber-wireless channel was presented in Chapter 1. In this chapter, a system model is discussed along with some critical issues. The relationship between the practical implementation of the fiber-wireless channel and the corresponding mathematical system is shown in Figure 2.1. The fiber-wireless channel consists of an 'ROF' link (which can be characterized by a nonlinearity) followed by the 'Air' transmission medium (which can be characterized by a CIR reflecting the multipath dispersion). Figure 2.1 represents the fiber-wireless downlink (base station → user), in the uplink (user → base station) the two systems are reversed.

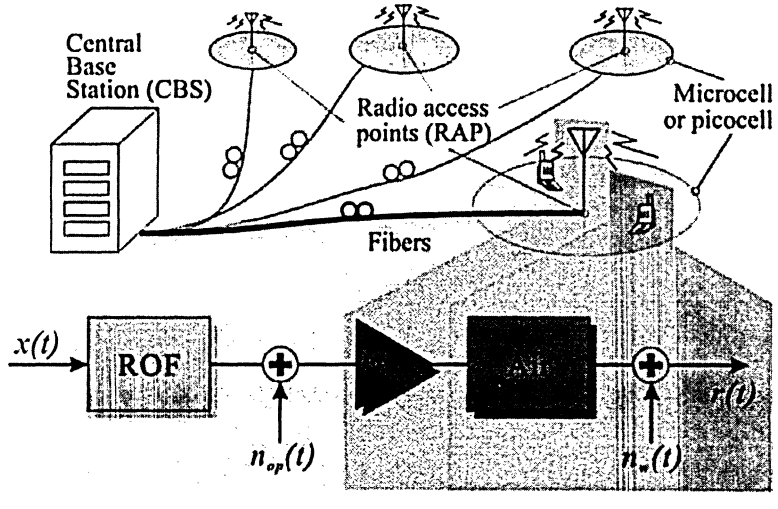

Figure 2.1: Block diagram representation of the fiber-wireless system [9].

2.2 Issues with the fiber-wireless system

Dominant issues in the fiber-wireless channel are discussed in detail in this section.

2.2.1 Wireless channel distortion

Two important distortions resulting from the wireless channel include ISI and MAI.

ISI: ISI is caused by multipath propagation and results in the spreading of a transmitted pulse over time. Depending on the environment, the multipath propagation can either be severe or mild.

MAI: When multiple users are transmitted via the wireless channel each user acts as interference to all other users and vice versa. MAI is a major issue and its effects cannot be neglected.

Dynamic range is also a concern. This is true more so in the uplink than the downlink. In the uplink, the received signal first travels through the wireless channel, resulting in path losses, fading and shadowing (due to obstructions), before entering the optical fiber; this makes the dynamic range of the input very large.

Of course, as with any other medium, the input signal is distorted to a certain degree by the addition of noise. Noise is random and unpredictable and can come from many sources. Examples of external noise include man-made noise, fluorescent lights, and natural noise such as lightning. Internal noise comes from electronic circuitry in the transmitter and receiver.

2.2.2 Nonlinearity

One of the major issues with the fiber-wireless channel is the nonlinear distortion of the optical (ROF) link. This is due mainly to the laser diode, and partly to the high-gain RF amplifier at the optical receiver. The nonlinear nature of the optical source is shown in Figure 2.2. There is a limited linear region and eventually the output optical power saturates. The nonlinearity of the laser diode can be expressed by the polynomial

$$P = D + P_a(S + D_2S^2 + D_3S^3), \tag{2.1}$$

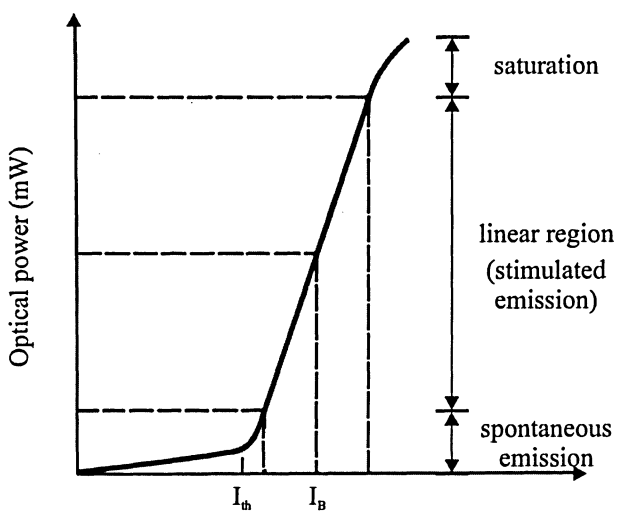

Figure 2.2: Laser nonlinearity.

where P is the output optical power, S is the modulating current signal, P_a is the average transmitted optical power, and D, D_2 and D_3 are constants determined by the laser diode such as the optical modulation depth. Furthermore, the nonlinearity of the laser can be affected by factors such as leakage current and temperature variations.

Experimental measurements on the **combined** nonlinearity of the ROF link are shown in Figure 2.3. This figure shows the output RF power from the optical receiver versus the input RF power into the laser. It is clear that the output power is a nonlinear function of the input power, in large part due to the laser diode and would be even more pronounced with an amplifier in the system. The dynamic range requirement of the uplink in a typical microcellular environment is 80-90 dB, but the dynamic range available from a typical ROF link is about 20-30 dB less than the above requirement [10]. To satisfy this large dynamic range, the nonlinearity must be characterized in order to apply adequate compensation. This is especially important in a multiuser environment where the number of users is dynamic.

According to the theorem of Weierstrass [11], any function which is continuous within an interval may be approximated to any required degree of accuracy by polynomials in this interval. From Figures 2.2 and 2.3 it is clear that the nonlinearity follows a saturating characteristic and can therefore be modelled using a third order memoryless polynomial ([12],

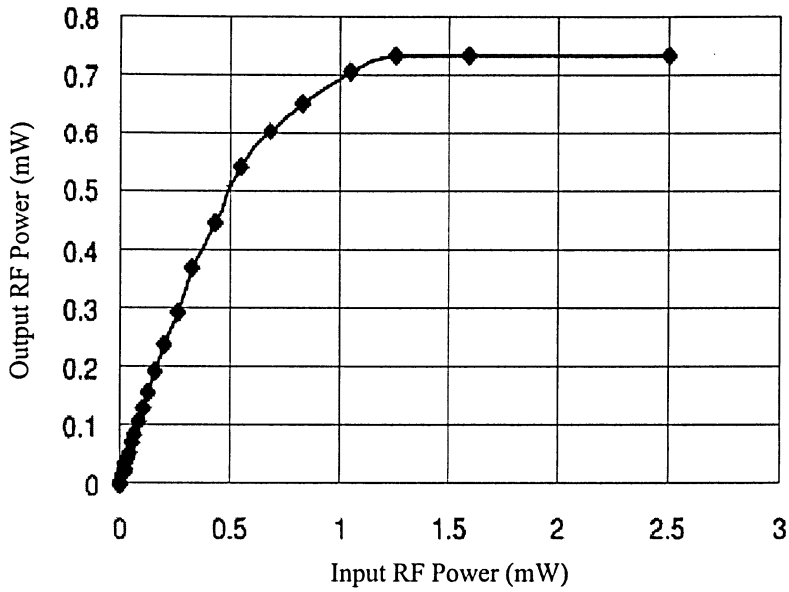

Figure 2.3: ROF link nonlinearity.

[13], [7]). However, the modelling of the nonlinearity should be done on Figure 2.3 because this relates the input power to the output power. Two important observations regarding the output of a nonlinear system in the passband can be made from [14] and [15], they are:

1. only odd order terms contribute to the system output, and
2. even order terms appear out of band and can easily be filtered out.

Taking into consideration the above, the ROF link nonlinearity can be approximated by a third order polynomial of the form

$$y = c_1 x^3 + c_2 x, \tag{2.2}$$

where adjusting the coefficients c_1 and c_2 lead to different saturating characteristics. There is no constant term in equation (2.2) because in most practical applications if there is no input there is no output. For our case this is justified in Figure 2.3.

2.2.3 Optical receiver noise

Optical receiver noise is another concern. Either PIN or avalanche photodiode (APD) type detectors are used in optical receivers. PIN photodetectors are used in ROF because they

perform better at wavelengths of 1310 nm and 1550 nm [4]. Therefore, only the noise issues for a PIN photodetector will be discussed. Photodetector noises in the receiver arise from the statistical nature of the photon-to-electron conversion process, and thermal noises come from the amplifier circuitry [12]. Two important noises in the optical receiver are described below.

Shot noise: Comes from the incoming photon stream. This noise occurs because of the random nature of the production and collection of photoelectrons when an optical signal is incident on a photodetector. The expression for shot noise can be written as

$$\langle i_{shot}^2 \rangle = 2qI_pB, \tag{2.3}$$

where q is the charge of an electron, I_p is the average value of the photocurrent, and B is the bandwidth.

Thermal noise: Comes from the bias resistor and is directly proportional to the temperature. The expression for thermal noise is given as

$$\langle i_T^2 \rangle = \frac{4k_BT}{R_L}B, \tag{2.4}$$

where k_B is Boltzmann's constant, T is the absolute temperature in Kelvin, and R_L is the load resistance.

2.2.4 Relative intensity noise

Changes in the amplitude or intensity of the output of a laser produce optical intensity noise. These changes can either be due to temperature variations or from spontaneous emissions. The noise resulting from these random intensity fluctuations is called relative intensity noise (RIN) [12]. The mean square value of the RIN noise current is given by

$$\langle i_{RIN}^2 \rangle = P_{RIN}\Re^2P_0^2B, \tag{2.5}$$

where P_{RIN} is the relative intensity noise parameter in dB/Hz, $\Re$ is the responsivity, and P_0 is the mean optical power.

2.3 Nonlinear system theory

This section deals with the mathematical modelling of the fiber-wireless channel. Modelling dynamic systems with linear models is difficult because linear models only approximate the system behaviour around a *given operating point.* However, modelling dynamic systems with nonlinear models allows the behaviour of the system to be approximated over the *whole operating range.* But since the field of nonlinear systems is so huge, it is difficult to characterize all nonlinear systems with one model structure. The selection of a nonlinear model depends on the application.

In our case it is already known that the fiber-wireless channel consists of the series connection of a linear dynamic system with a static nonlinearity. This type of nonlinearity can be modelled using a block-oriented structure. It has been shown in many applications (see [16] and the references therein) that block-oriented models can successfully represent a wide range of nonlinear systems. For example, block-oriented models have been successfully used in the areas of:

- chemical processes,
- biological processes,
- satellite communications, and
- control systems.

Some of the more common types of block-oriented models are: 1) Feedback block-oriented, 2) Wiener, and 3) Hammerstein. The Wiener and Hammerstein block-oriented models consist of the interconnection of a linear time invariant (LTI) system with a static memoryless nonlinearity and are shown in Figure 2.4. Aside from the fact that our channel is dynamic, these structures are ideal for modelling the fiber-wireless link. But in order to get a communication system oriented model, multiple users, as well as wireless and optical channel noise must be considered. In the next section, the theory for the basic Wiener and Hammerstein systems will be discussed. In Chapter 4, this theory will be extended to a multiuser communications environment.

2.3.1 Volterra series

The Wiener and Hammerstein models are shown in Figures 2.4(a) and 2.4(b), respectively. These are special cases of the Wiener-Hammerstein model of Figure 2.4(c). The following two similarities between the system models in Figure 2.4 and the fiber-wireless communication link can be made:

1. the Wiener model is analogous to the fiber-wireless uplink, and
2. the Hammerstein model is analogous to the fiber-wireless downlink.

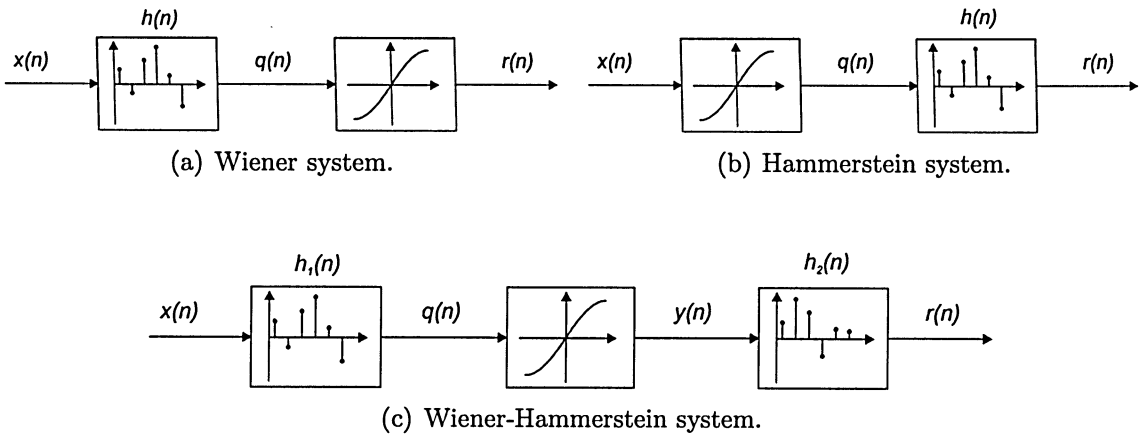

(a) Wiener system.

(b) Hammerstein system.

(c) Wiener-Hammerstein system.

Figure 2.4: Wiener and Hammerstein models for series connection of linear systems with static memoryless nonlinearities.

Wiener and Hammerstein systems provide a convenient means to model the fiber-wireless channel and fortunately extensive mathematical analysis has been done with these systems. These models have been thoroughly analyzed in a single control signal (or single user) continuous-time baseband environment ([17], [8], [11], [18]).

The input-output relationship of a nonlinear system with memory is given in [19] and [20] in continuous-time. Converting to discrete-time, the relationship can be given by the following Volterra series

$$r(n) = h_0 + \sum_{m_1=-\infty}^{\infty} h_1(m_1)x(n-m_1) + \sum_{m_1=-\infty}^{\infty}\sum_{m_2=-\infty}^{\infty} h_2(m_1,m_2)x(n-m_1)x(n-m_2) + \ldots + \sum_{m_1=-\infty}^{\infty}\cdots\sum_{m_n=-\infty}^{\infty} h_n(m_1,\ldots,m_n)x(n-m_1)\ldots x(n-m_n), \quad (2.6)$$

where $h_n(m_1, ..., m_n)$ are called the Volterra kernels of the system. Just as an LTI system can be completely characterized by its impulse response, so can a nonlinear system, which can be represented by a Volterra series, be completely characterized by its Volterra kernels [21]. It can also be shown [19], using a similar argument to that for linear systems, that a nonlinear system is causal if and only if

$$h_n(m_1, ..., m_n) = 0, \quad \text{for any } m_j < 0, \tag{2.7}$$

where $j = 1, ..., n$. Equation (2.6) is a very general definition, and hence the Volterra kernels vary depending on the mathematical structure of the nonlinearity. The Volterra series and kernels for the case when the nonlinearity is given by a polynomial of order l will be discussed next.

Wiener system

The output of the linear channel in Figure 2.4(a) can be written as

$$q(n) = h(n) * x(n) = \sum_{m=-\infty}^{\infty} h(m)x(n-m). \tag{2.8}$$

Then, the output of the nonlinear system can be represented by a polynomial of the form

$$r(n) = F[q(n)] = A_1 q(n) + A_2 q^2(n) + ... + A_l q^l(n), \tag{2.9}$$

where $A_1, A_2, ..., A_l$ are the polynomial coefficients and l is the highest order of the polynomial. By substituting for $q(n)$ in the above equation, the system output can be expressed by the following discrete-time Volterra series

$$r(n) = A_1 \sum_{m_1=-\infty}^{\infty} h(m_1)x(n-m_1) + A_2 \sum_{m_1=-\infty}^{\infty} \sum_{m_2=-\infty}^{\infty} h(m_1)h(m_2)x(n-m_1)x(n-m_2)$$
$$+ ... + A_l \sum_{m_1=-\infty}^{\infty} ... \sum_{m_l=-\infty}^{\infty} \prod_{i=1}^{l} h(m_i)x(n-m_i). \tag{2.10}$$

The output $r(n)$ consists of an input $x(n)$ that has been dispersed in time due to the impulse response and subsequently raised to higher order powers due to the nonlinearity. The output can also be written as a summation of the output of the isolated l^{th} order kernel as

$$r(n) = w_1(n) + w_2(n) + ... + w_l(n), \tag{2.11}$$

where

$$w_l(n) = A_l \sum_{m_1=-\infty}^{\infty} \dots \sum_{m_l=-\infty}^{\infty} \prod_{i=1}^{l} h(m_i)x(n-m_i). \tag{2.12}$$

Comparing equations (2.6) and (2.10) (and substituting g_p for h_n to avoid confusing notation), the Volterra kernels $g_p(m_1, m_2, ..., m_p)$ for a Wiener system can be found to be

$$g_p(m_1, m_2, ..., m_p) = A_p \sum_{\tau=-\infty}^{\infty} \prod_{i=1}^{p} h(m_i - \tau). \tag{2.13}$$

This general definition takes into account a memory term τ, however, we assume our nonlinearity to have no memory and hence the memory term is excluded in our derivation. In general, the output of the isolated l^{th} order kernel for a Wiener system can be written as

$$w_l(n) = \sum_{m_1=-\infty}^{\infty} \dots \sum_{m_l=-\infty}^{\infty} g_l(m_1, m_2, ..., m_l) \prod_{i=1}^{l} x(n-m_i). \tag{2.14}$$

The Volterra series and kernels for the Hammerstein system are discussed next.

Hammerstein system

In the case of Figure 2.4(b), the output of the nonlinear channel is given by

$$q(n) = F[x(n)] = A_1x(n) + A_2x^2(n) + \dots + A_lx^l(n), \tag{2.15}$$

and the output of the linear system can be represented by a convolution of the form

$$r(n) = h(n) * q(n) = \sum_{m=-\infty}^{\infty} h(m)q(n-m). \tag{2.16}$$

By substituting for $q(n)$ in the above equation, the system output can be expressed by the following discrete-time Volterra series

$$r(n) = A_1 \sum_{m=-\infty}^{\infty} h(m)x(n-m) + A_2 \sum_{m=-\infty}^{\infty} h(m)x^2(n-m) + \dots + A_l \sum_{m=-\infty}^{\infty} h(m) \prod_{i=1}^{l} x(n-m). \tag{2.17}$$

The output consists of an input that has been raised to higher order powers and subsequently dispersed in time. The output can also be written as a summation of the output of the isolated l^{th} order kernel as

$$r(n) = w_1(n) + w_2(n) + ... + w_l(n). \tag{2.18}$$

Comparing equations (2.6) and (2.17) (and again substituting g_p for h_n), the Volterra kernels $g_p(m)$ for a Hammerstein system are simply given as

$$g_p(m) = A_p h(m). \tag{2.19}$$

The above theory provides a foundation onto which the extension into the multiuser domain can be done.

2.4 Spread spectrum communications

This section provides a brief overview on spread spectrum communications and a comprehensive overview of spreading sequences. Spread spectrum techniques are widely used in the communications industry. In CDMA, a communication channel with a certain bandwidth is accessed by all users simultaneously. This is achieved by spreading the baseband signal bandwidth over a larger bandwidth by introducing a higher frequency signal (or code) [22]. At the receiver, the same code that was used in spreading the information is used to perform an operation called despreading, which recovers the original data signal in its original bandwidth. Some advantages to spread spectrum communications include:

- antijamming capabilities,
- interference rejection,
- low probability of interception and detection,
- privacy through secure communication, and
- ability to provide multiple access (CDMA).

One of the most important aspects of spread spectrum systems is the code embedded in the information signal. This code can be utilized in a variety of ways, each resulting in a different spread spectrum technique. In direct sequence spread spectrum (DSSS) the spreading code is inserted at the data level, in frequency hopping spread spectrum (FHSS) the spreading code acts at the carrier-frequency level, and in time hopping spread spectrum (THSS) the spreading code acts as an on/off gate to the transmitted signal ([23], [24]).

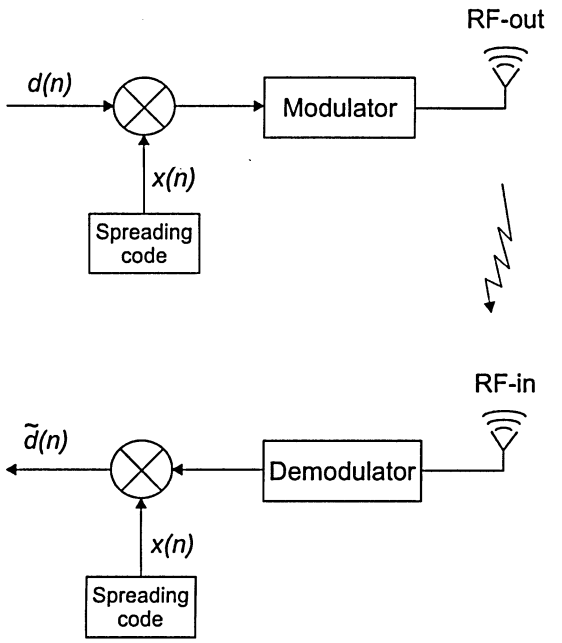

(a) Spreading the data signal.

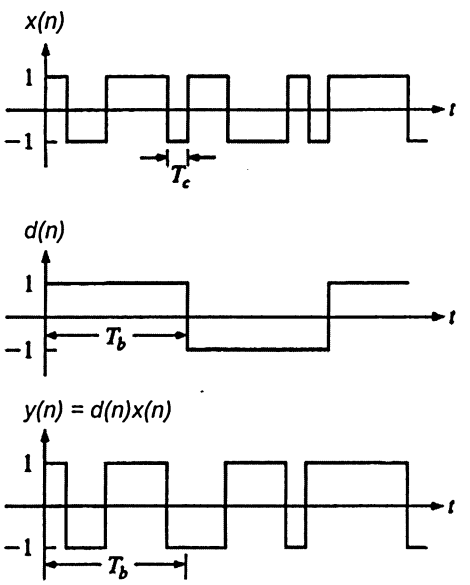

(b) **Top:** spreading sequence, **Middle:** data signal, **Bottom:** spread signal.

Figure 2.5: DSSS communications.

An example of DSSS follows. In this scheme, the spreading is done by multiplying the input data by a spreading sequence whose bit rate is much higher than that of the data rate. The data signal, given by $d(n)$ in Figure 2.5, is expressed as

$$d(n) = \sum_{k=-\infty}^{\infty} d_k g_{T_b}(n - kT_b), \tag{2.20}$$

where $d_k = \pm 1$ and $g_{T_b}(n)$ is a rectangular pulse of duration T_b. In order to spread the data signal, it is multiplied by a spreading sequence given by

$$x(n) = \sum_{k=-\infty}^{\infty} x_k p_{T_c}(n - kT_c), \tag{2.21}$$

where x_k is the spreading sequence (in this case it is a sequence of ± 1's) and $p_{T_c}(n)$ is a rectangular pulse of duration T_c. The multiplication of $d(n)$ and $x(n)$ spreads the bandwidth of the data signal from $1/T_b$ Hz into a much wider bandwidth of $1/T_c$ Hz. The resultant signal is

$$y(n) = \sum_{k=-\infty}^{\infty} y_k r_{T_c}(n - kT_c), \tag{2.22}$$

where y_k is the product $d_k x_k$ and $r_{T_c}(n)$ is a rectangular pulse of duration T_c. The processing gain is defined as

$$PG = \frac{BW[y(n)]}{BW[d(n)]}, \tag{2.23}$$

where $BW[y(n)] \gg BW[d(n)]$.

The code used in spreading the spectrum is an integral part of the system. Prior to transmission, the transmitter and receiver must have knowledge of which code is used. In the event that the wrong code is used for despreading, the received data will be useless. The idea is to generate a sequence that appears random to the channel but is reproducible at the receiver. This ensures that the aforementioned benefits of spread spectrum will hold true. The bit pattern of a truly random sequence never repeats, and in order to retain this characteristic it is desirable for the user generated code to be as long as possible and as random as possible. Generation of a sequence with these properties is difficult and would have little use in a practical system. The idea is to generate a semi-random sequence or a pseudo-random bit sequence (PRBS). Some of the more popular PRBS sequences are: PN (or m-sequences), Gold, Kasami, and Hadamard-Walsh. Each of these codes can be classified according to various properties. The more important properties are run length, autocorrelation, cross correlation, and orthogonality.

As mentioned in the previous chapter, the spreading sequences utilized for estimation in this thesis are **PN sequences** and **Walsh codes**. For the purposes of identification it is essential that the correlation properties of these sequences be well understood, especially in a multiuser environment. The remainder of this chapter discusses these properties.

2.4.1 Pseudonoise sequences

PN sequences can either be classified as maximal length (m-sequences) or non-maximal length. The sequences that have received the most attention are maximal length sequences, because, as the name suggests, they are sequences of maximum possible period generated from a linear feedback shift register (LFSR). Properties of non-maximal sequences are generally poor compared to those of maximal sequences, and so m-sequences are usually much preferred over their non-maximal counterparts. The LFSR generator polynomial dictates whether or not the sequence reaches its maximum possible period before repeating. Galois field mathematics can be used to derive the feedback taps that provide this condition. When referring to PN sequences in the rest of this thesis, they will always be of maximal length.

PN sequences have well defined correlation properties ([25], [26], [27]). The properties of maximal length PN sequences are summarized below:

Length: The length of a PN sequence is given by

$$N_c = 2^n - 1, \tag{2.24}$$

where n $\equiv$ degree of generating polynomial. The PN sequence is periodic, repeating every N_c samples.

Monopolar/Bipolar: The sequence can be defined in terms of 0's and 1's or ± 1's. The formula given by

$$b = (-1)^m = 1 - 2m \tag{2.25}$$

can be used to convert from monopolar to bipolar and vice versa. m refers to the monopolar value and b refers to the bipolar value.

Balance: The number of 1's and 0's differs only by one, with there being an additional 0 for the monopolar case and an additional 1 for the bipolar case.

Autocorrelation: One of the most important properties of a PN sequence is its periodic autocorrelation. The periodic autocorrelation of the PN sequence $x(n)$ can be defined as

$$\Re_{xx}(\sigma) = E[(x(n)x(n-\sigma)] = \overline{x(n)x(n-\sigma)}, \tag{2.26}$$

which gives one of two cases [26]

$$\Re_{xx}(\sigma) = \begin{cases} N_c & \text{if } \sigma = 0 \\ -1 & \text{if } \sigma \neq 0 \end{cases}, \tag{2.27}$$

when the autocorrelation is taken over the period $0 \leq n \leq N_c - 1$. Clearly, the autocorrelation properties of maximal-length PN sequences are very good. It is important to have this optimal autocorrelation otherwise there will be multiple identifications, one at each autocorrelation peak. Also, multiple identifications would make it difficult to separate the actual impulse response from the erroneous impulse response peaks.

Cross correlation: The cross correlation of the PN sequences $x(n)$ and $y(n)$ can be defined as

$$\Re_{xy}(\sigma) = E[(x(n)y(n-\sigma)] = \overline{x(n)y(n-\sigma)}. \tag{2.28}$$

For system identification purposes, it is important that the sequence family posses low cross correlation so as to minimize the interaction between users. Using independent PN sequences, i.e. each sequence is generated using a different LFSR generating polynomial, ensures that the cross correlation is minimized. However, the cross correlation properties of PN sequences are still limited when compared to the good autocorrelation property. It was shown in [26] that PN sequences can have relatively large cross correlation peaks as presented in Table 2.1. These maximum cross correlations are the worst case scenarios. Numerical analysis showed that the peak cross correlations of the PN sequences used for the simulations in this thesis had much smaller peak values than those shown in Table 2.1.

Example: PN sequence

The purpose of this small section is to show a PN sequence that satisfies all of the above properties. A 4^{th} order PN sequence is given by

$$[1 \quad -1 \quad -1 \quad -1 \quad 1 \quad 1 \quad 1 \quad 1 \quad -1 \quad 1 \quad -1 \quad 1 \quad 1 \quad -1 \quad -1], \tag{2.29}$$

which has a length of $N_c = 2^4 - 1 = 15$. It is a bipolar sequence that satisfies the balance property (8 ones and 7 negative ones). The autocorrelation of this PN sequence is given in

n	N_c	Number of PN sequences	Maximum peak cross correlation
3	7	2	5
4	15	2	9
5	31	6	11
6	63	6	23
7	127	18	41
8	255	16	95
9	511	48	113
10	1023	60	383
11	2047	176	287
12	4095	144	1407
13	8191	630	$\geq$ 703

Table 2.1: Peak cross correlation of PN sequences.

Figure 2.6. The autocorrelation property is satisfied because at the zeroth lag the amplitude is 15 (N_c), whereas at all other lags the amplitude is -1.

2.4.2 Walsh codes

Walsh codes are used in the downlink of CDMA systems because of their orthogonality property and hence good correlation properties when synchronized. In the downlink, transmission is synchronous, and as long as the Walsh codes are orthogonal they do not interfere with one another. The despreading operation works best under this condition. Orthogonal codes are used in systems where the receiver is perfectly synchronized with the transmitter. The base station transmits a pilot signal to help the receiver gain synchronization.

Walsh codes have the following properties:

Length: The length (or period) of a Walsh code is given by N_w, where N_w is a power of 2. The code index, which is an integer scalar in the range $[0, 1, ..., N_w - 1]$, specifies the number of zero crossings in the output.

Autocorrelation: The autocorrelation, at zero lag ($\sigma = 0$), of the Walsh code $x(n)$ can be defined as

$$\Re_{xx}(0) = E[(x(n)x(n)] = \overline{x(n)x(n)} = N_w. \tag{2.30}$$

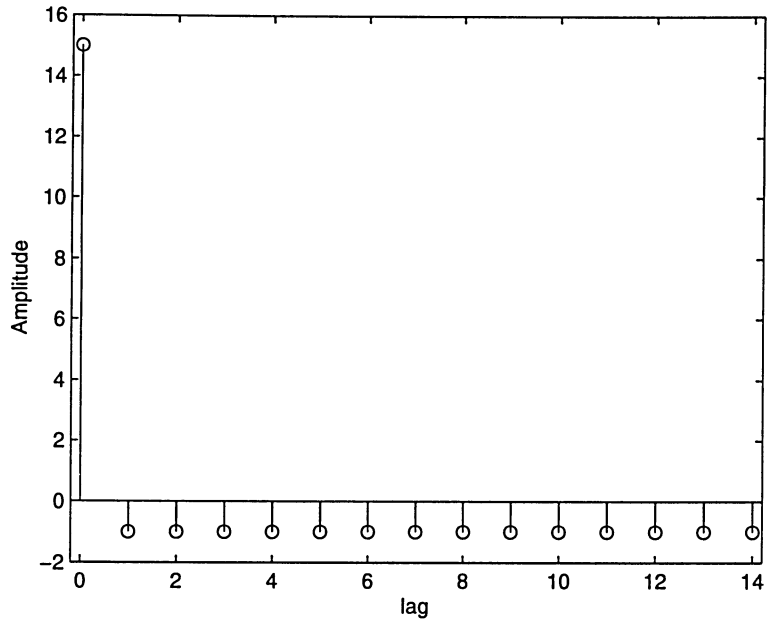

Figure 2.6: PN sequence autocorrelation.

Cross correlation: The cross correlation, at zero lag ($\sigma = 0$), of the Walsh codes $x(n)$ and $y(n)$ can be defined as

$$\Re_{xy}(0) = E[(x(n)y(n)] = \overline{x(n)y(n)} = 0. \tag{2.31}$$

Unfortunately, Walsh codes do not have as well defined correlation properties as PN sequences, other than during synchronization. In contrast, Walsh codes can have relatively large autocorrelation and cross correlation peaks at non-zero lags ([28], [29]). Studying Walsh codes theoretically can prove to be difficult, but studying Walsh codes through simulations is an effective way to analyze their correlation properties. Simulations of Walsh code correlations will be discussed graphically in Chapter 6. It will be shown, through the use of simulations, that Walsh codes can indeed be used for estimation purposes under certain conditions.

Chapter 3

Related work on identification of block-oriented models

Several approaches have been developed in the literature to identify Wiener and Hammerstein (or block-oriented) nonlinear systems. One of the most important conclusions that was made upon reviewing the literature was that current methods fail to address the problem of estimation in an environment where a parallel connection of multiple linear systems is encountered in series with a single nonlinearity. All Wiener/Hammerstein identification methods were performed with either *single signals* or with multiple input single output (MISO) block-oriented systems [30]. The problem with MISO systems is that there are multiple nonlinear channels in addition to multiple linear channels. This results in system dynamics that are very different from the situation where the summation of multiple signals is sent through a single nonlinearity. Even though there hasn't been literature published on fiber-wireless system identification specifically, it is still useful to discuss other approaches for the single user case. The three main approaches for single user Wiener/Hammerstein system identification are based on:

- iterative techniques,
- orthonormal bases, and
- correlation analysis.

Some additional techniques involving subspace, frequency domain, and neural network approaches will also be discussed.

3.1 Iterative techniques

Narendra *et al.* [31] developed an iterative procedure for identification of a **Hammerstein** system. The parameters of the linear system and the coefficients of the polynomial are alternately adjusted to minimize a mean square error (MSE) criterion. The optimal values for one system are calculated while fixing the parameters of the other system. The output of the nonlinearity of the Hammerstein system in Figure 2.4(b) is given by the polynomial

$$q(n) = F[x(n)] = A_1 x(n) + A_2 x^2(n) + ... + A_l x^l(n), \tag{3.1}$$

and the linear channel is denoted by the transfer function

$$H(z) = a_0 + a_1 z^{-1} + ... + a_{n-1} z^{-(n-1)}. \tag{3.2}$$

The coefficients $A_1, A_2, ..., A_l$ and $a_0, a_1, ..., a_{n-1}$ are adjusted to minimize $\sum_j e_j^2$ where e_j denotes the error at time j between the output of the system and the model output. The summation is carried out over the total number of input and output samples. The steps of the algorithm are outlined below:

1. The linear approximation of $H^{(1)}(z)$ is obtained by using the input-output records of the linear system along with the iterative algorithm referred to in [31].

2. The coefficients of the nonlinear system $A_1, A_2, ..., A_l$ are calculated by minimizing a mean square criteria. Since the input $x(n)$ is known, the updated signal $q^{(2)}(n)$ can also be calculated once the polynomial coefficients are estimated.

3. Using the signal $q^{(2)}(n)$, an updated approximation of the linear system $H^{(2)}(z)$ is obtained by repeating step 1. The process is continued for as many iterations as needed to satisfy the error criterion.

Access to the internal signal $q(n)$ was assumed in this approach. However, in the fiber-wireless communication system there is no access to this signal.

Korenberg *et al.* [32] developed an iterative technique for the **Wiener** system of Figure 2.4(a). The algorithm is used in a single signal biomedical setting. The advantage of this

technique is that the estimation can be done when the record length is relatively short. The algorithm comprises the following steps:

1. Estimate $h(n)$ from the best dynamic linear fit between $x(n)$ and $r(n)$.

2. Estimate $q(n)$ from the convolution $q(n) = \sum_{m=-\infty}^{\infty} h(m)x(n-m)$.

3. Best fit a polynomial between the estimate of $q(n)$ and $r(n)$.

4. Use the inverse of the estimated polynomial, with $r(n)$ as the input, to obtain a new estimate of $q(n)$.

5. Re-estimate $h(n)$ from the best dynamic linear fit between $x(n)$ and the updated $q(n)$.

6. Re-estimate $q(n)$ from the convolution $q(n) = \sum_{m=-\infty}^{\infty} h(m)x(n-m)$.

7. Either go to step 3 (another iteration) or go to step 8 (final estimate).

8. Best fit a polynomial between the latest $q(n)$ estimate and $r(n)$.

The iterative techniques described above only consider noise distortion at the output. They do not analyze the effects of any distortion on the internal signal $q(n)$. Therefore, no conclusions are made regarding the robustness of the algorithms in the presence of multiple error terms. It is desirable to be able to estimate the system using PN sequence inputs, however, Korenberg *et al.* stayed away from using white noise-like inputs because of the requirement for a large record length. If the record length is not sufficiently large then the estimates of the linear and nonlinear elements in the Wiener model can have significant inaccuracies [32]. Consequently, Korenberg *et al.* described an iterative procedure that can enhance the accuracy of estimating a Wiener model when the record length is relatively short, and that effectively corrects for the restriction on the input to be white noise-like [32]. The iterative algorithm has the advantage of efficiency, however convergence can be a concern.

3.2 Orthonormal bases

Gómez *et al.* [16] provide a comprehensive treatment on noniterative algorithms for the identification of Wiener and Hammerstein systems based on orthonormal functions. *A priori* information of the system dynamics is available during system identification by representing the linear and nonlinear systems with orthonormal functions. In terms of basis functions, the nonlinearity can be written as

$$F[q(n)] = \sum_{i=1}^{r} a_i f_i(q(n)), \tag{3.3}$$

where a_i are unknown matrix parameters. The nonlinear functions f_i are generally polynomials which allows for the representation of smooth nonlinearities, but they can also be radial basis functions or basis functions generated by translations and dilations of a mother function (e.g. wavelets) [16]. The linear system can be written in terms of the basis functions as

$$H(q) = \sum_{l=0}^{p-1} b_l B_l(q), \tag{3.4}$$

where q is the forward shift operator, b_l are unknown matrix parameters, and $B_l(q)$ are rational orthonormal bases functions. The identification problem is to estimate the unknown parameter matrices a_i (i = 2, ..., r) (a_1 is taken to be equal to the identity matrix) and b_l (l = 0, ..., p-1) from recorded input-output measurements.

Defining $\theta \triangleq [a_2, a_3, ..., a_r, b_0, b_1, ..., b_{p-1}]$, Φ as a matrix containing the basis functions, and Y as the system output, the steps of the algorithm for identification of the **Wiener** system are:

1. Compute the least squares estimate of θ by using the equation $\hat{\theta} = (\Phi_N \Phi_N^T)^{-1} \Phi_N Y_N$.

2. Compute estimates of the matrices a and b by partitioning $\hat{\theta}$ obtained in step 1.

The **Hammerstein** identification algorithm is based on a least squares and singular value decomposition (SVD) approach. The linear and nonlinear systems are defined the same as for the Wiener model (equations (3.4) and (3.3), respectively). The steps for the Hammerstein system identification are:

1. Compute the least squares estimate $\hat{\theta}$ using the equation $\hat{\theta} = (\Phi_N \Phi_N^T)^{-1} \Phi_N Y_N$, where Φ is a matrix containing the basis functions and Y is the system output. Then find the matrix $\hat{\Theta}_{ab}$ by using $\hat{\theta}$ and the block column matrix approach as in Section 2.2 of [16].

2. Compute the SVD of $\hat{\Theta}_{ab}$ and the partition of this decomposition.

3. Compute the estimates of the parameter matrices a and b using the above decomposition of $\hat{\Theta}_{ab}$.

$\hat{\Theta}_{ab}$ and θ are defined as

$$\hat{\Theta}_{ab} \triangleq \begin{bmatrix} a_1^T b_0^T & a_1^T b_1^T & \dots & a_1^T b_{p-1}^T \\ a_2^T b_0^T & a_2^T b_1^T & \dots & a_2^T b_{p-1}^T \\ \vdots & \vdots & \dots & \vdots \\ a_r^T b_0^T & a_r^T b_1^T & \dots & a_r^T b_{p-1}^T \end{bmatrix}, \quad \text{and} \quad \theta \triangleq [b_0 a_1, \dots, b_0 a_r, \dots, b_{p-1} a_1, \dots, b_{p-1} a_r]^T. \quad (3.5)$$

There is obviously more depth to the algorithm than what was presented above. The algorithm is presented in broad terms because the intention of this section is just to give a general overview. The reader is referred to [16] for details.

Neural network approach

Fang *et al.* [33] used an orthogonal wavelet-based neural network (OWNN) to identify a **Wiener system**. A linear auto regressive moving average (ARMA) model was used to model the linear subsystem and an OWNN was used to model the static nonlinear subsystem. In terms of modelling the static nonlinearity, different kinds of neural networks such as the multilayer feedforward neural network, radial basis functions, and wavelet networks can be used because of their well-known ability to approximate nonlinear functions [33]. In Fang *et al.*'s approach, the OWNN architecture is simplified and a simple learning method is used to search for the optimum neural network weights. A few iterations of the back-propagation algorithm and a QR-decomposition-based optimal technique were used in the neural network learning method. Wavelets were used as the basis for the othonormal functions.

Let the structure of the linear system and nonlinearity in Figure 2.4(a) be given as

$$q(n) = \sum_{i=1}^{n} a_i q(n-i) + \sum_{j=0}^{m} b_j x(n-j), \text{ and} \tag{3.6}$$

$$r(n) = F[q(n)], \tag{3.7}$$

respectively. The goal of the identification algorithm is to appropriately adjust the coefficients of the ARMA model and the weights of the OWNN. The internal signal $q(n)$ is not available for measurement, and so the coefficients of the ARMA model are first estimated using the RLS algorithm. A small input signal is used for this part of the estimation to ensure that the nonlinear system operates in the linear range. The amplitude of the input signal is then increased and the weights of the OWNN are determined. The steps of the algorithm are outlined below:

1. Initialize the ARMA model and apply a small input signal to the system. Record the output.

2. Use the RLS algorithm to identify the coefficients of the ARMA model.

3. Increase the amplitude of the input signal and apply it to both the ARMA model and the system. Use a combination of the back-propagation algorithm and QR-decomposition to learn the weights of the OWNN (for details on this refer to Section III of [33]).

3.3 Correlation analysis

Correlation analysis techniques for Wiener ([8], [11], [18]) and Hammerstein [34] system identification have been extensively studied by Billings *et al.*. In the aforementioned papers, correlation analysis was used to decouple the identification of the linear and nonlinear component subsystems. The identification was done by using maximal-length PN sequences which satisfied the requirement for an input with white noise-like properties (i.e. an impulse-like autocorrelation function). It is on the work of Billings *et al.* that much of the work in this thesis is based upon, so at this point a discussion of correlation analysis techniques is put off until Chapter 4.

3.4 Other techniques

Frequency domain identification

Bai identified a Wiener and Hammerstein model in the frequency domain in [35] and [36], respectively. Frequency domain identification is based on analyzing the fundamental frequency and harmonics generated by an unknown nonlinearity. By exploring the frequencies contained in the output, the phase of the unknown transfer function can be calculated based on discrete Fourier transforms of the sampled output. Then, the nonlinearity as well as the magnitude of the linear part can be estimated. Consider the **Wiener** system in Figure 2.4(a). Let the transfer function $H(s)$ represent the unknown linear system and $F(.)$ represent the unknown nonlinearity. In order to perform frequency domain identification, the input

$$x(t) = A\cos(\omega_k t) \tag{3.8}$$

is applied to the system, where $k = 1, 2, ..., q$, and for some value of A. The goal is to determine a pair of estimates so that

$$\hat{F}[.] \rightarrow F[.], \quad \text{and} \quad \hat{H}(j\omega_k) \rightarrow H(j\omega_k). \tag{3.9}$$

No *a priori* information on the structure of $F(.)$ is assumed. The only requirement for the unknown nonlinearity is that it be continuous and piecewise smooth. Bai justifies this restriction by saying that many nonlinearities encountered in practice can either be characterized by polynomials, or have a saturating or dead-zone characteristic. Frequency domain identification is particularly useful when knowledge about the system before identification is so poor that the family of all possible characteristics cannot be parameterized [35]. A drawback of the algorithm is that it has to be run as many times as the number of frequencies q.

The **Hammerstein** identification is done in a similar manner as for the Wiener system. For specifics the reader is referred to [36].

Subspace methods

Subspace-based state-space system identification methods have been successfully used in identifying LTI systems. Gomez *et al.* [37] expanded subspace identification from LTI systems to that of block-oriented systems. The idea is to use a subspace-based method to estimate the system matrices of the linear model and then to perform an SVD in order to separately estimate the nonlinear and linear matrix coefficients. The subspace-based approach requires modest computational complexity and is more robust than correlation based techniques. There has been gaining interest in this area and an idea for future work is to examine how the subspace-based approach performs in identifying a multiuser fiber-wireless CDMA communication link.

Chapter 4

Fiber-wireless uplink estimation using PN sequences

Fiber-wireless uplink estimation in three different CDMA scenarios is considered in this chapter, they are:

1. single user,
2. multiuser with a common wireless channel for each user (MUc), and
3. multiuser with a different wireless channel for each user (MU).

Of the three scenarios presented above, the lattermost has the most practical value and so more emphasis is put on analyzing that case (specifically in the simulations of Section 4.7). The theory for each scenario will be discussed with the help of nonlinear systems theory. Since a thorough analysis of the single user case (neglecting noise) was presented in Section 2.3, only the major variations from that single user case will be discussed with respect to the above three cases. Before proceeding with the estimation theory, a short section regarding complex notation will be discussed.

4.1 Passband complex consideration

Communication signals and systems are passband. In order to use baseband signal processing, communication signals in the passband (i.e. real-valued signals [22]), must be appropriately translated from the passband to the baseband. Generally, this translation results

in complex-valued baseband signals [22]. Therefore, in a fiber-wireless passband system, the signals, as well as the CIR and nonlinear component are complex-valued. We now show how these complex-valued quantities can be split into real-valued quadrature components.

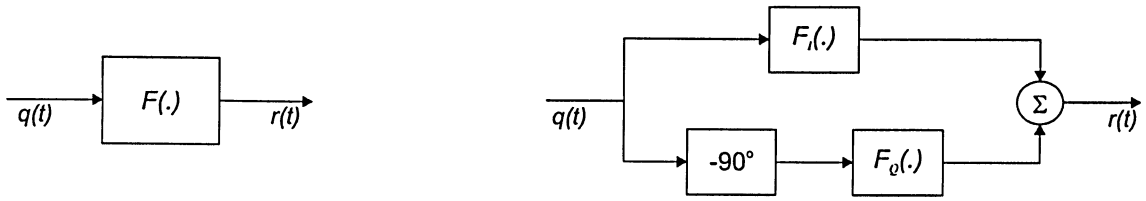

(a) Single complex-valued system.

(b) Two real-valued systems.

Figure 4.1: Inphase and quadrature phase model for a complex nonlinear system.

When an RF signal undergoes a nonlinear transformation one of the major concerns is the AM-AM and AM-PM distortions. The complex-valued nonlinear fiber link in Figure 4.1(a) introduces both of these distortions [10]. It has been shown in [38] and [4] that a bandpass memoryless nonlinearity can be modelled with a baseband complex nonlinear model. Then, the nonlinear distortion can be expressed by inphase and quadrature phase components that are real. Let the input signal in Figure 4.1(a) be given as

$$q(t) = A(t)cos[\omega_c t + \theta(t)]. \tag{4.1}$$

Then the output $r(t)$ is

$$r(t) = R[A(t)]cos\{\omega_c t + \theta(t) + \phi[A(t)]\}, \tag{4.2}$$

where R is the AM-AM distortion and ϕ is the AM-PM distortion. The output $r(t)$ can also be expressed as

$$r(t) = R[A(t)]cos(\phi[A(t)])cos(\omega_c t + \theta(t)) - R[A(t)]sin(\phi[A(t)])sin(\omega_c t + \theta(t)), \tag{4.3}$$

using the trigonometric identity $cos(A+B) = cos(A)cos(B) - sin(A)sin(B)$. Equation (4.3) can then be written as

$$r(t) = r_p[A(t)]cos(\omega_c t + \theta(t)) - r_q[A(t)]sin(\omega_c t + \theta(t)), \tag{4.4}$$

where

$$r_p[A(t)] = R[A(t)]cos(\phi[A(t)]) \tag{4.5}$$

$$r_q[A(t)] = R[A(t)]sin(\phi[A(t)]). \tag{4.6}$$

Equation (4.4) shows that the bandpass nonlinearity can be separated into an inphase component and a quadrature phase component with only AM-AM distortion. Therefore, the two real-valued systems shown by the quadrature model in Figure 4.1(b) are equivalent to the complex-valued system shown in Figure 4.1(a). Similarly, the bandpass CIR can also be separated into inphase and quadrature phase components [22].

Mathematically, real quantities are easier to work with and therefore the quadrature model is the representation of choice in this thesis. As a result of this, it can be stated that for both the linear and nonlinear systems in this thesis, the real-valued inphase and quadrature phase components are estimated individually. All variables introduced hereafter are real quantities unless otherwise specified.

4.2 Single user CDMA environment

Continuing with the estimation theory. The most basic fiber-wireless communication system is that of a single user. In such a case, there is no MAI from other users and the limitations to successful estimation are multipath dispersion, nonlinearities, and wireless and optical channel noise. The block diagram of Figure 4.2 depicts the fiber-wireless uplink in a single user CDMA environment. This block diagram represents one branch in the architecture of

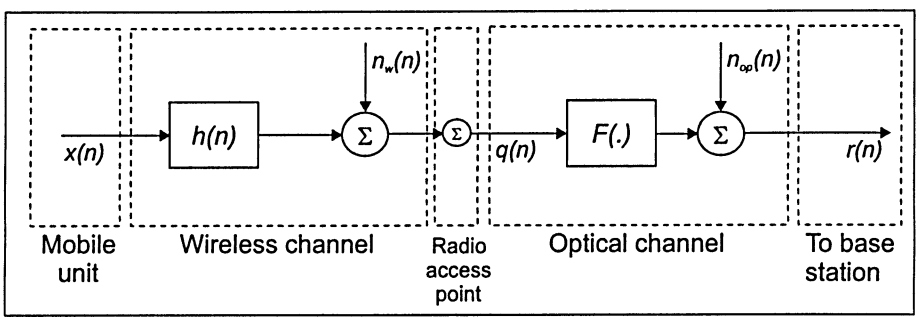

Figure 4.2: Fiber-wireless uplink in a single user CDMA environment.

Symbol	Description
$x_j(n)$	input PN spreading sequence, $1 \leq j \leq N$
$u(n)$	compound PN signal input
$h_j(n)$	wireless channel impulse response, $1 \leq j \leq N$
$n_{w(j)}(n)$	wireless channel Gaussian noise, $1 \leq j \leq N$
$q(n)$	signal sent to optical channel
$F(\cdot)$	optical channel nonlinear function
$n_{op}(n)$	optical receiver Gaussian noise
$r(n)$	signal sent to central base station

Table 4.1: Symbol descriptions for fiber-wireless uplink.

Figure 1.1. The wireless channel noise is added after the wireless channel and the optical channel noise is added at the optical link receiver; both noise sources are Gaussian. The RAP is shown in Figure 4.2 simply as a summation–the RAP has more relevance in the multiuser case and is included here for purposes of continuity with the multiuser block diagrams. All signals used in analyzing the fiber-wireless uplink, along with their descriptions, are shown in Table 4.1. These symbols will be relevant for this single user case and forthcoming multiuser cases as well.

The first step in estimating the single user fiber-wireless uplink is to define the output of the system. Using the theory presented in Section 2.3, the system output in Figure 4.2 can be written as

$$r(n) = \sum_{k=1}^{l} A_k \Big(\sum_{m_1=-\infty}^{\infty} \cdots \sum_{m_k=-\infty}^{\infty} \prod_{i=1}^{k} h(m_i)x(n-m_i) + n_w^k(n) \Big) + \text{ CMT } + n_{op}(n), \quad (4.7)$$

where the cross multiplied terms (CMT) can be found using the multinomial theorem [39] with 2 terms and l^{th} order. Refer to appendix A for a discussion on the multinomial theorem. The output can also be written as a summation of the output of the isolated l^{th} order kernel as

$$r(n) = w_1(n) + w_2(n) + \ldots + w_l(n) + n_{op}(n), \quad (4.8)$$

where CMT is included in the terms $w_1(n), w_2(n), \ldots, w_l(n)$. By studying the correlation between the output $r(n)$ and the input $x(n)$, as well as the output of the 1^{st} order kernel $w_1(n)$ and the input $x(n)$, the linear and nonlinear channels can be estimated. But before

analyzing the correlation relationships, the system outputs of the other two multiuser cases will be presented.

4.3 Multiuser CDMA environment with a common wireless channel

Identification of the fiber-wireless channel in a single user CDMA environment yields the best results; however, transmission of only one users signal through the fiber-wireless channel is not very practical. Extending the theory for the single user case to a multiuser environment can yield a much more useful application of the estimation algorithm. The theory developed in this section, and proceeding sections, shows that the fiber-wireless uplink can be identified, to a certain degree of accuracy, in a CDMA communication system where all users transmit their signal simultaneously. However, as the number of users increases, MAI becomes a major concern that must be removed in order to succeed with the identification.

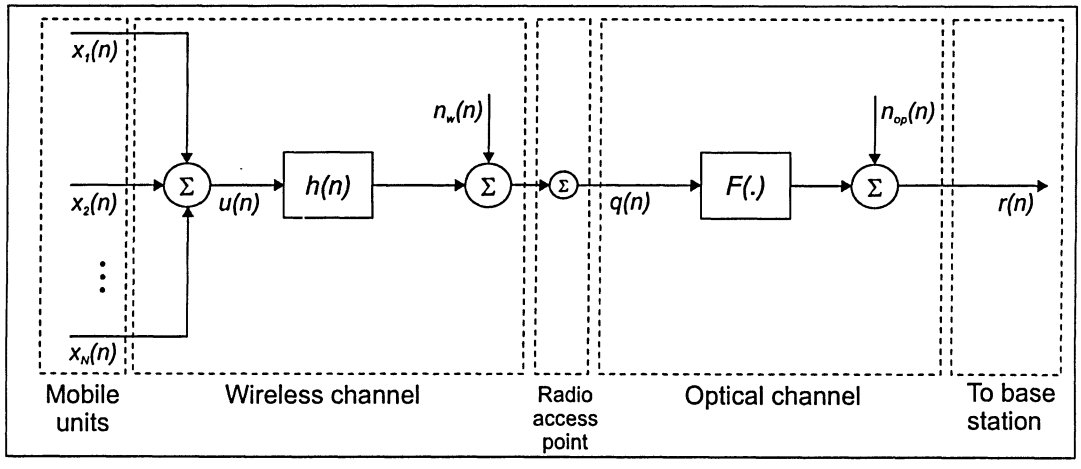

Figure 4.3: Fiber-wireless uplink in a multiuser CDMA environment with a common wireless channel.

The scenario of a multiuser CDMA environment with a common wireless channel is shown in Figure 4.3.[1] This sort of environment may be encountered in a restricted scenario where users are in a cluster and therefore has practical limitations. It is considered here for

[1]The common wireless channel is allowed due to the distributive law for convolution. For example, instead of having each user transmit through the same wireless channel, i.e. $\{x_1(n) * h(n) + x_2(n) * h(n)\}$, the summation of all users can be transmitted through one wireless channel, i.e. $\{[x_1(n) + x_2(n)] * h(n)\}$.

completeness. For this case, the input is a compound input consisting of the summation of multiple users PN sequences. The compound input is given as

$$u(n) = x_1(n) + x_2(n) + ... + x_N(n), \tag{4.9}$$

where N is the number of PN sequences and hence the number of users. The multiple PN sequences are independent of each other. In other words, each is generated using a different LFSR polynomial. The signal at the RAP in Figure 4.3 is given as

$$q(n) = \Big(\sum_{j=1}^{N} x_j(n)\Big) * h(n) + n_w(n) = u(n) * h(n) + n_w(n). \tag{4.10}$$

After the nonlinear channel, by substituting for $q(n)$, the output of the fiber-wireless uplink is

$$\begin{aligned} r(n) &= \sum_{k=1}^{l} A_k q^k(n) + n_{op}(n) \\ &= \sum_{k=1}^{l} A_k \Big(u(n) * h(n) + n_w(n)\Big)^k + n_{op}(n). \end{aligned} \tag{4.11}$$

Further utilizing the Volterra series representation and expanding the convolution gives the final output as

$$r(n) = \sum_{k=1}^{l} A_k \Big(\sum_{m_1=-\infty}^{\infty} ... \sum_{m_k=-\infty}^{\infty} \prod_{i=1}^{k} h(m_i)u(n-m_i) + n_w^k(n)\Big) + \text{ CMT } + n_{op}(n). \tag{4.12}$$

Similar to equation (4.7), the output can also be written as a summation of the output of the isolated l^{th} order kernel as

$$r(n) = w_1(n) + w_2(n) + ... + w_l(n) + n_{op}(n), \tag{4.13}$$

where CMT is included in the terms $w_1(n), w_2(n), ..., w_l(n)$ and can be found using the multinomial theorem with 2 terms and l^{th} order.

4.4 Multiuser CDMA environment with separate wireless channels

The scenario of a multiuser CDMA environment with separate wireless channels is shown in Figure 4.4. In this scenario: 1) each user generates an independent PN sequence, 2)

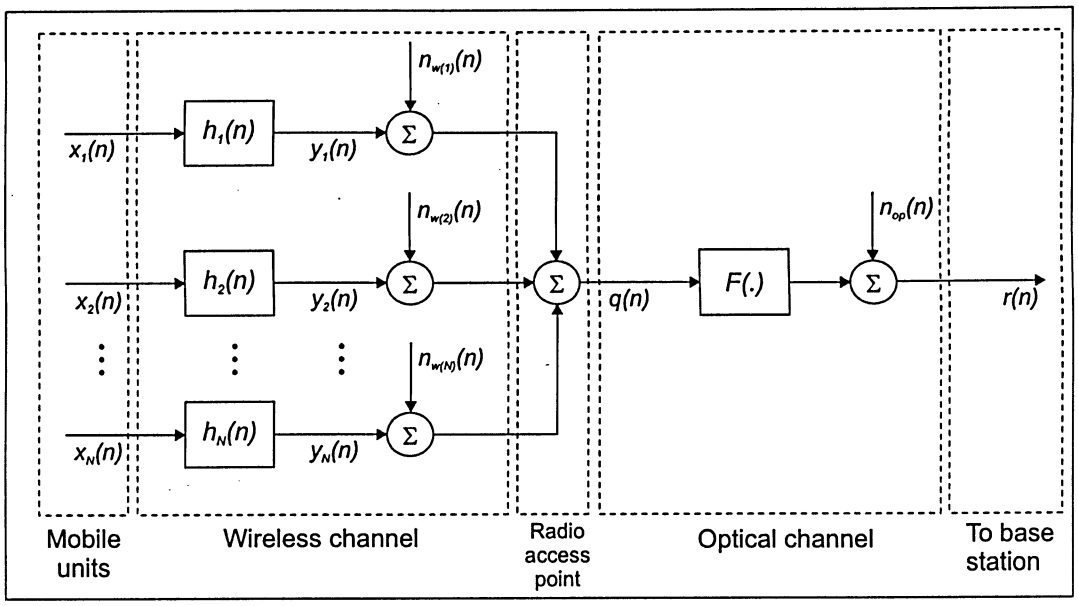

Figure 4.4: Fiber-wireless uplink in a multiuser CDMA environment with separate wireless channels.

transmits through a separate wireless channel followed by the addition of an independent wireless channel noise[2], 3) multiple users are then combined and transmitted through the nonlinear optical link followed by the addition of optical receiver noise, and finally 4) the combined signal is sent to the central base station for further processing. This scenario generates a multitude of signal impairments, particularly because of transmission through the many wireless channels. Impairments include: 1) ISI from the wireless channels, 2) different path loss affecting dynamic range, 3) addition of wireless and optical channel noise, 4) MAI at the RAP, 5) carrier regrowth, inband distortion, and cross multiplication of terms, all resulting from the nonlinear optical link.

Taking the summation of all wireless channels at the RAP in Figure 4.4 gives

$$q(n) = \sum_{j=1}^{N} [x_j(n) * h_j(n) + n_{w(j)}(n)]. \tag{4.14}$$

[2]Different 'initial seed' settings are used during simulation to ensure independence.

After the nonlinear channel, the output of the fiber-wireless uplink is

$$\begin{aligned} r(n) &= \sum_{k=1}^{l} A_k q^k(n) + n_{op}(n) \\ &= \sum_{k=1}^{l} A_k \Big(\sum_{j=1}^{N} [x_j(n) * h_j(n) + n_{w(j)}(n)] \Big)^k + n_{op}(n), \end{aligned} \tag{4.15}$$

giving the final output as

$$r(n) = \sum_{k=1}^{l} A_k \Big\{ \sum_{j=1}^{N} \Big(\sum_{m_1=-\infty}^{\infty} \cdots \sum_{m_k=-\infty}^{\infty} \prod_{i=1}^{k} h_j(m_i) x_j(n-m_i) + n^k_{w(j)}(n) \Big) \Big\} + \text{ CMT } + n_{op}(n), \tag{4.16}$$

where CMT can be found using the multinomial theorem with $[2 \times N]$ terms and l^{th} order. The output can also be written as a summation of the output of the isolated l^{th} order kernel as

$$r(n) = w_1(n) + w_2(n) + ... + w_l(n) + n_{op}(n), \tag{4.17}$$

where CMT is included in the terms $w_1(n), w_2(n), ..., w_l(n)$. It may seem repetitive to keep mentioning that the output can be written as equation (4.17), however, expressing the output in this manner is a crucial step in developing the correlation relationships that follow.

4.5 Correlation relationships

The next step in the estimation of the fiber-wireless channel is to further process the input-output relations, as defined above, by utilizing correlation relationships. Only the correlation relationships for the MUc and MU case are developed. It is straightforward to extend the theory from these more complex cases to the simpler single user case.

4.5.1 Input-output correlation

The expression for the input-output correlation can be generalized for all three cases under the condition that the output $r(n)$ is expressed by equations (4.8), (4.13), and (4.17). A commonly defined input is used in the derivation, given by $z(n)$, where

- $z(n) = x(n)$ in the single user case,

- $z(n) = u(n)$ in the MUc case, and
- $z(n) = x_j(n)$ in the MU case.

Using the general input $z(n)$ and the output $r(n)$, along with equation (2.28), the cross covariance between them can be written as

$$\Re_{zr}(\sigma) = \overline{(r(n) - \overline{r(n)})(z(n-\sigma) - \overline{z(n-\sigma)})}. \tag{4.18}$$

The cross covariance relationship is used extensively throughout this section. From this point onward $r(n)$, $u(n)$, $q(n)$, $n_{op}(n)$, $z(n)$, and $x_j(n)$, $n_{w(j)}(n)$ for $1 \leq j \leq N$ will refer to their respective signals with the mean removed. In some cases [11], a mean level is added to the input PN sequence to ensure that all terms in equations (4.8), (4.13), and (4.17) contribute to the 1st order input-output cross correlation. However, in this case, only the output of the 1st order kernel is of interest (discussed shortly) and hence a mean level is not needed. With means removed, the cross covariance can be written as

$$\Re_{zr}(\sigma) = \overline{r(n)z(n-\sigma)}. \tag{4.19}$$

Substituting equation (4.17) into the above equation and simplifying gives

$$\begin{aligned}
\Re_{zr}(\sigma) &= \overline{[w_1(n) + w_2(n) + ... + w_l(n) + n_{op}(n)][z(n-\sigma)]} \\
&= \overline{w_1(n)z(n-\sigma) + w_2(n)z(n-\sigma) + ... + w_l(n)z(n-\sigma) + n_{op}(n)z(n-\sigma)} \\
&= \overline{w_1(n)z(n-\sigma)} + \overline{w_2(n)z(n-\sigma)} + ... + \overline{w_l(n)z(n-\sigma)} + \overline{n_{op}(n)z(n-\sigma)} \\
&= \Re_{zw_1}(\sigma) + \Re_{zw_2}(\sigma) + ... + \Re_{zw_l}(\sigma) + \Re_{zn_{op}}(\sigma),
\end{aligned} \tag{4.20}$$

which can be written in a more compact form as

$$\Re_{zr}(\sigma) = \sum_{k=1}^{l} \Re_{zw_k}(\sigma) + \Re_{zn_{op}}(\sigma). \tag{4.21}$$

Assuming the input PN sequence and noise process to be statistically independent, i.e. $\overline{n_{op}(n)z(n-\sigma)} = 0 \; \forall \; \sigma$, the term $\Re_{zn_{op}}(\sigma)$ becomes negligible. Equation (4.21) then becomes

$$\Re_{zr}(\sigma) = \sum_{k=1}^{l} \Re_{zw_k}(\sigma), \tag{4.22}$$

however, if $\Re_{zr}(\sigma)$ is evaluated directly as defined above, the terms $\sum_{k=2}^{l} \Re_{zw_k}(\sigma)$ give rise to anomalies associated with multidimensional autocovariances of PN sequences [8]. This problem can be overcome by isolating $\Re_{zw_1}(\sigma)$ using multilevel input testing. It should be noted that if the channel were linear there would be no need to isolate $\Re_{zw_1}(\sigma)$ because $\Re_{zw_1}(\sigma) = \Re_{zr}(\sigma)$.

Multilevel testing enables the extraction of $\Re_{zw_1}(\sigma)$ from $\Re_{zr}(\sigma)$. This step is crucial for successful estimation of the wireless channel. Multilevel testing is implemented at the RAP by using the signal $\alpha_m q(n)$, where $\alpha_m \neq \alpha_l \ \forall \ m \neq l$, and repeating l times. For example, with a 3rd order nonlinearity the output of the MU system can be written as

$$\begin{aligned} r(n) &= A_1 q(n) + A_2 q^2(n) + A_3 q^3(n) + n_{op}(n) \\ &= w_1(n) + w_2(n) + w_3(n) + n_{op}(n). \end{aligned} \tag{4.23}$$

With the multilevel input $\alpha_1 q(n)$, the above equation becomes

$$\begin{aligned} r_{\alpha_1}(n) &= A_1\alpha_1 q(n) + A_2\alpha_1^2 q^2(n) + A_3\alpha_1^3 q^3(n) + n_{op}(n) \\ &= \alpha_1 w_1(n) + \alpha_1^2 w_2(n) + \alpha_1^3 w_3(n) + n_{op}(n), \end{aligned} \tag{4.24}$$

which when used to find $\Re_{zr}(\sigma)$ gives the following modified form of equation (4.22)

$$\boxed{\Re_{zr_{\alpha_m}}(\sigma) = \sum_{k=1}^{l} \alpha_m^k \Re_{zw_k}(\sigma), \quad m = 1, 2, ..., l}, \tag{4.25}$$

where r_{α_m} is the response of the system to multilevel inputs. An important condition when using multilevel inputs is that the number of multilevel inputs used be equal to the highest polynomial order. This ensures that the algorithm works in the presence of any order nonlinear function. Representing equation (4.25) in matrix form gives

$$\begin{bmatrix} \Re_{zr_{\alpha_1}}(\sigma) \\ \Re_{zr_{\alpha_2}}(\sigma) \\ . \\ . \\ \Re_{zr_{\alpha_l}}(\sigma) \end{bmatrix} = \begin{bmatrix} \alpha_1 & \alpha_1^2 & . & . & \alpha_1^l \\ \alpha_2 & \alpha_2^2 & . & . & \alpha_2^l \\ . & . & . & . & . \\ . & . & . & . & . \\ \alpha_l & \alpha_l^2 & . & . & \alpha_l^l \end{bmatrix} \begin{bmatrix} \Re_{zw_1}(\sigma) \\ \Re_{zw_2}(\sigma) \\ . \\ . \\ \Re_{zw_l}(\sigma) \end{bmatrix}. \tag{4.26}$$

To check the above α matrix for singularities, it is divided into two matrices as follows

$$\begin{bmatrix} \alpha_1 & 0 & . & . & 0 \\ 0 & \alpha_2 & 0 & . & 0 \\ . & 0 & . & . & 0 \\ . & . & . & . & . \\ 0 & 0 & . & . & \alpha_l \end{bmatrix} \begin{bmatrix} 1 & \alpha_1 & \alpha_1^2 & . & \alpha_1^{l-1} \\ 1 & \alpha_2 & \alpha_2^2 & . & \alpha_2^{l-1} \\ . & . & . & . & . \\ . & . & . & . & . \\ 1 & \alpha_l & \alpha_l^2 & . & \alpha_l^{l-1} \end{bmatrix}. \tag{4.27}$$

The matrix on the left hand side (LHS) of equation (4.27) is clearly nonsingular for $\alpha_m \neq 0$. The matrix on the right hand side (RHS) of equation (4.27) is the Vandermonde matrix which has a non-zero determinant given by

$$\prod_{1 \leq i < j \leq l} (\alpha_j - \alpha_i), \tag{4.28}$$

for $\alpha_i \neq \alpha_j$. Therefore, for every value of σ, equation (4.26) has a unique solution for $\Re_{zw_i}(\sigma)$, $i = 1, 2, ..., l$. Now that $\Re_{zw_1}(\sigma)$ (the input-kernel correlation) can be extracted, the final step in the identification process is to find how $\Re_{zw_1}(\sigma)$ relates to the CIR.

4.5.2 Input-kernel correlation for MUc case

In this section $z(n) = u(n)$. In order to accommodate for multiple PN sequences, as well as wireless and optical channel noise, the covariance relationship in [8] had to be reworked. Initially the input-kernel cross covariance $\Re_{x_1 x_2 ... x_N w_N}(\sigma)$ was derived, however this result was undesirable because of the dependency on higher order kernels w_N, and hence multidimensional autocovariances. Another approach was to consider the cross covariance between the compound input $u(n)$ and $w_1(n)$, given as

$$\Re_{uw_1}(\sigma) = \overline{w_1(n)u(n-\sigma)}. \tag{4.29}$$

Replacing $w_1(n)$ using the information from equations (4.12) and (4.13) and expanding the input $u(n)$ gives

$$\Re_{uw_1}(\sigma) = \overline{A_1\Big(\sum_{m_1=-\infty}^{\infty} h(m_1)[x_1(n-m_1) + x_2(n-m_1) + ... + x_N(n-m_1)] + n_w(n)\Big)} \; \overline{\Big([x_1(n-\sigma) + x_2(n-\sigma) + ... + x_N(n-\sigma)]\Big)}. \tag{4.30}$$

Another possibility for the above covariance was to consider the cross covariance between $w_1(n)$ and individual users inputs, instead of the compound input $u(n)$. However, it was found through simulations that using the compound input gave more accurate results. The reason being that a compound input gives N terms where two identical PN sequences are correlated, compared to only one term when individual inputs are used. Overall, having N terms results in better covariance properties as will be shown by the next equation. Expanding and simplifying equation (4.30) gives

$$\Re_{uw_1}(\sigma) = A_1 \sum_{m_1=-\infty}^{\infty} h(m_1)[\Re_{x_1x_1}(m_1-\sigma)+\Re_{x_2x_2}(m_1-\sigma)+...+\Re_{x_Nx_N}(m_1-\sigma)+\Re_{x_1n_w}(\sigma) + \Re_{x_2n_w}(\sigma)+...+\Re_{x_Nn_w}(\sigma)+\text{CMT}]. \quad (4.31)$$

It is interesting to note that the optical noise term n_{op} is not present in the above equation. However, n_{op} indirectly introduces error into the above expression via the multilevel testing extraction process. During the extraction, the optical noise present in $\Re_{ur}(\sigma)$ introduces error into the extracted term $\Re_{uw_1}$.

Three different types of terms can be observed by examining equations (4.30) and (4.31):

1. $\Re_{x_ix_{j,j=i}}(m_1-\sigma)$, the covariance between two identical PN sequences,
2. $\Re_{x_ix_{j,j\neq i}}(m_1-\sigma)$, the covariance between two different PN sequences (CMT), and
3. $\Re_{x_jn_w}(\sigma)$, the covariance between a PN sequence and wireless channel noise,

where $1 \leq i,j \leq N$. The outcome of the first case is the autocovariance, whose properties were discussed in Section 2.4.1. As mentioned above, using a compound input gives the summation of N autocovariance terms. This yields a large autocovariance value and hence improves the accuracy of identification. The outcome of the second case is the cross covariance. When compared to the large autocovariance value, the cross covariance can be considered negligible. The outcome of the third case was again taken to be negligible by assuming the input and noise process to be statistically independent. Applying all the aforementioned approximations gives

$$\Re_{uw_1}(\sigma) = A_1 \sum_{m_1=-\infty}^{\infty} h(m_1)[\Re_{x_1x_1}(m_1-\sigma)+\Re_{x_2x_2}(m_1-\sigma)+...+\Re_{x_Nx_N}(m_1-\sigma)]. \quad (4.32)$$

Using the relationship $\Re_{x_i x_i}(\lambda) = N_c \delta_i(\lambda)$ and the convolution properties of the impulse function gives

$$\begin{aligned}\Re_{uw_1}(\sigma) &= A_1 N_c \sum_{m_1=0}^{N_c-1} h(m_1)[\delta_1(m_1-\sigma) + \delta_2(m_1-\sigma) + ... + \delta_N(m_1-\sigma)] \\ &= A_1 N_c \sum_{i=1}^{N} h(\sigma). \end{aligned} \tag{4.33}$$

Therefore, the final cross covariance relationship can be written as

$$\boxed{\Re_{uw_1}(\sigma) = A_1 N_c N h(\sigma)}, \tag{4.34}$$

where N is the number of PN sequences, N_c is the PN sequence length, and A_1 is the linear gain of the nonlinear system. The estimated CIR can be found by solving the above expression.

4.5.3 Input-kernel correlation for MU case

In this section $z(n) = x_j(n)$. Using the input $x_1(n)$ (i.e. the channel of interest will be that of the first user in all following derivations) and the output of the 1st order kernel $w_1(n)$, the cross covariance between them can be written as

$$\Re_{x_1 w_1}(\sigma) = \overline{w_1(n) x_1(n-\sigma)}. \tag{4.35}$$

Replacing $w_1(n)$ using the information from equations (4.16) and (4.17) gives

$$\Re_{x_1 w_1}(\sigma) = \overline{\Big\{A_1 \sum_{j=1}^{N} \Big(\sum_{m_1=-\infty}^{\infty} h_j(m_1) x_j(n-m_1) + n_{w(j)}(n) \Big) \Big\} \Big\{ x_1(n-\sigma) \Big\}}. \tag{4.36}$$

The first few terms of the above equation are expanded below in order to get a clear picture of the covariances

$$\begin{aligned}\Re_{x_1 w_1}(\sigma) = A_1 \sum_{m_1=-\infty}^{\infty} \Big[& h_1(m_1) \overline{x_1(n-m_1) x_1(n-\sigma)} + h_2(m_1) \overline{x_2(n-m_1) x_1(n-\sigma)} \\ & + ... + h_N(m_1) \overline{x_N(n-m_1) x_1(n-\sigma)} \Big] + \overline{n_{w(1)}(n) x_1(n-\sigma)} \\ & + \overline{n_{w(2)}(n) x_1(n-\sigma)} + ... + \overline{n_{w(N)}(n) x_1(n-\sigma)}. \end{aligned} \tag{4.37}$$

Simplifying the above equation gives

$$\Re_{x_1 w_1}(\sigma) = A_1 \sum_{m_1=-\infty}^{\infty} \Big[h_1(m_1)\Re_{x_1 x_1}(m_1 - \sigma) + h_2(m_1)\Re_{x_1 x_2}(m_1 - \sigma) + \ldots + h_N(m_1) \Re_{x_1 x_N}(m_1 - \sigma) \Big] + \Re_{x_1 n_{w(1)}}(\sigma) + \Re_{x_1 n_{w(2)}}(\sigma) + \ldots + \Re_{x_1 n_{w(N)}}(\sigma). \tag{4.38}$$

Ideally, only the term $\Re_{x_1 x_1}(m_1 - \sigma)$ would be present on the RHS of the above equation and the identification of the wireless channel would be complete. However, in a multiuser environment there are two different types of additional terms, they are:

1. $[N]$ cross covariance terms of the form $\Re_{x_1 n_{w(j;1 \leq j \leq N)}}(\sigma)$, and
2. $[N-1]$ additional cross covariance terms of the form $\Re_{x_1 x_{j;2 \leq j \leq N}}(m_1 - \sigma)$.

The outcome of the first case is simply the cross covariance between the desired users input with each wireless channel noise. These terms can be taken negligible by assuming the input and noise process to be statistically independent. However, with additional users, even these noise terms can cause problems in the identification. The practical limitation of our scheme in terms of signal-to-noise ratio (SNR) will be discussed in Section 4.7.

The outcome of the second case is the cross covariance between the desired users input with all other users inputs. This is a major source of interference, i.e. MAI, and it must be mitigated in order to end up with an accurate identification. As the number of users increases, MAI becomes an increasingly large error term that hinders the identification. MAI mitigation can be done in one of two ways:

1. by using longer PN sequences to improve the covariance relationships, or
2. by using an iterative technique to remove MAI.

The first solution would be easy, however not very practical. The second solution is what is proposed in this thesis. With knowledge of the initial CIR estimates, an iterative technique is developed to minimize the effect of MAI. The steps for the iterative algorithm are described below:

Iterative algorithm

Step 1: Run simulation algorithm. This gives access to $x_1(n)...x_N(n)$, $r(n)$ (MAI inclusive) and initial CIR estimates $\tilde{h}_1^{(1)}(n)...\tilde{h}_N^{(1)}(n)$.

Step 2: Using initial/updated CIR estimates and known PN inputs, approximate the signals entering the RAP, $\tilde{y}_1(n)...\tilde{y}_N(n)$, by convolution (refer to Figure 4.5).

Step 3: To isolate a user, subtract all *linear* MAI from the corrupted output $r(n)$ using the above estimates. For example, the MAI reduced outputs for users 1 and 2 are

$$\tilde{r}(n) = r(n) - (\tilde{y}_2(n) + \tilde{y}_3(n) + ... + \tilde{y}_N(n)), \text{ and} \tag{4.39}$$

$$\tilde{r}(n) = r(n) - (\tilde{y}_1(n) + \tilde{y}_3(n) + ... + \tilde{y}_N(n)), \tag{4.40}$$

respectively. This gives a better estimate of the output for each user, less other users MAI.

Step 4: Using the covariance between each users input PN sequence $x_1(n)...x_N(n)$, and their respectively reduced MAI outputs $\tilde{r}(n)$, find an updated CIR estimate $\tilde{h}_1^{(p)}(n)...\tilde{h}_N^{(p)}(n)$, where p is the number of iterations.

Step 5: Either go to step (2) to perform another iteration, or go to step (6) (CIR estimation is complete).

Step 6: Proceed to optical channel estimation.

It should be noted that in step (3) above, the estimated *linear* MAI is always subtracted from the corrupted output found in step (1). This way, a progressively larger amount of MAI is removed from the corrupted output. Only the *linear* MAI need be subtracted because the output of the 1st order kernel $w_1(n)$ is extracted using multilevels. An advantage of the algorithm is that it not only improves the CIR estimate,

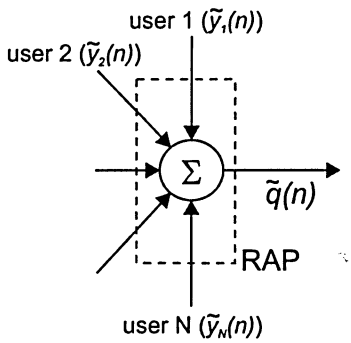

Figure 4.5: Estimation of internal signals.

but it also successfully removes erroneous peaks; more on this will be discussed in Section 4.7. A drawback of the iterative technique is that it requires a good initial estimate of the CIRs. In other words, the algorithm requires an initial estimate that has the general characteristics of the actual CIR. Therefore, as the number of users increases, the improvement in the estimation resulting from iterations starts to degrade. Additional processing time is also a concern.

Taking that MAI for user 1 is removed successfully and that the input and noise are statistically independent, equation (4.38) becomes

$$\Re_{x_1 w_1}(\sigma) = A_1 \sum_{m_1=-\infty}^{\infty} h_1(m_1) \Re_{x_1 x_1}(m_1 - \sigma). \tag{4.41}$$

Using the autocovariance property of PN sequences and the convolution properties of the impulse function, the above equation becomes

$$\Re_{x_1 w_1}(\sigma) = A_1 N_c \sum_{m_1=0}^{N_c-1} h_1(m_1) \delta_1(m_1 - \sigma) \tag{4.42}$$

$$\boxed{\Re_{x_1 w_1}(\sigma) = A_1 N_c h_1(\sigma)}, \tag{4.43}$$

giving the final cross covariance relationship. Where again, the estimated CIR can be found by solving the above expression.

4.6 Optical channel estimation theory

The optical channel is estimated by performing a least squares polynomial fit between the input and output of the nonlinear system. In the fiber-wireless channel there is no access to the internal signal $q(n)$ (the input to the nonlinear system) and therefore it must be estimated. Referring to Figure 4.4, this internal signal can be estimated by:

1. convolving the final CIR estimates $\tilde{h}_1^{(p)}(n)...\tilde{h}_N^{(p)}(n)$ (after p iterations) with their respective PN inputs $x_1(n)...x_N(n)$, and

2. summing the result over all users convolutions, giving the signal $\tilde{q}(n)$.

The least squares polynomial fit is then applied to the estimated signal $\tilde{q}(n)$ and the measured output $r(n)$.

Estimates of the polynomial coefficients can be made by using the aforementioned signals and an appropriate curve fitting algorithm. Let the estimated polynomial coefficients be given as

$$\hat{\mathbf{A}} = [\hat{A}_0 \quad \hat{A}_1 \quad \hat{A}_2 \quad . \quad . \quad . \quad \hat{A}_l]^T. \tag{4.44}$$

The estimated signal $\hat{r}(n)$ of the output of the nonlinear system is then given as

$$\hat{r}(n) = \hat{A}_0 + \hat{A}_1\tilde{q}(n) + \hat{A}_2\tilde{q}^2(n) + ... + \hat{A}_l\tilde{q}^l(n) + n_{op}(n). \tag{4.45}$$

The vectors $\tilde{\mathbf{q}}$ and $\mathbf{r}$ are defined as the signals $\tilde{q}(n)$ and $r(n)$, respectively. The Vandermonde matrix $\mathbf{V}$ can then be defined such that each row of $\mathbf{V}$ is a polynomial of the corresponding data point in $\tilde{\mathbf{q}}$. $\mathbf{V}$ is given by

$$\mathbf{V} = \begin{bmatrix} 1 & \tilde{q}(0) & \tilde{q}^2(0) & \tilde{q}^3(0) & . & \tilde{q}^l(0) \\ 1 & \tilde{q}(1) & \tilde{q}^2(1) & \tilde{q}^3(1) & . & \tilde{q}^l(1) \\ . & . & . & . & . & . \\ . & . & . & . & . & . \\ 1 & \tilde{q}(N_c-1) & \tilde{q}^2(N_c-1) & \tilde{q}^3(N_c-1) & . & \tilde{q}^l(N_c-1) \end{bmatrix}. \tag{4.46}$$

In matrix notation, the equation for a polynomial fit is given by

$$\hat{\mathbf{r}} = \mathbf{V}\hat{\mathbf{A}}. \tag{4.47}$$

Orthogonal-triangular (QR) decomposition was used to solve for $\hat{\mathbf{A}}$ in [7]. In this thesis, premultiplication is used. Premultiplying by the matrix transpose $\mathbf{V}^T$ and solving for $\hat{\mathbf{A}}$ gives

$$\hat{\mathbf{A}} = (\mathbf{V}^T\mathbf{V})^{-1}\mathbf{V}^T\hat{\mathbf{r}}. \tag{4.48}$$

The error between the actual data $\mathbf{r}$ and the estimated data $\hat{\mathbf{r}}$ is given by $e = \mathbf{r} - \mathbf{V}\hat{\mathbf{A}}$. The order of the polynomial l must be selected to minimize the MSE.

Once the CIRs have been estimated, the estimation of the nonlinear channel is straightforward. However, the accuracy of the nonlinear identification is highly dependent on the CIR estimates and so it is important that the CIR estimation algorithm work well.

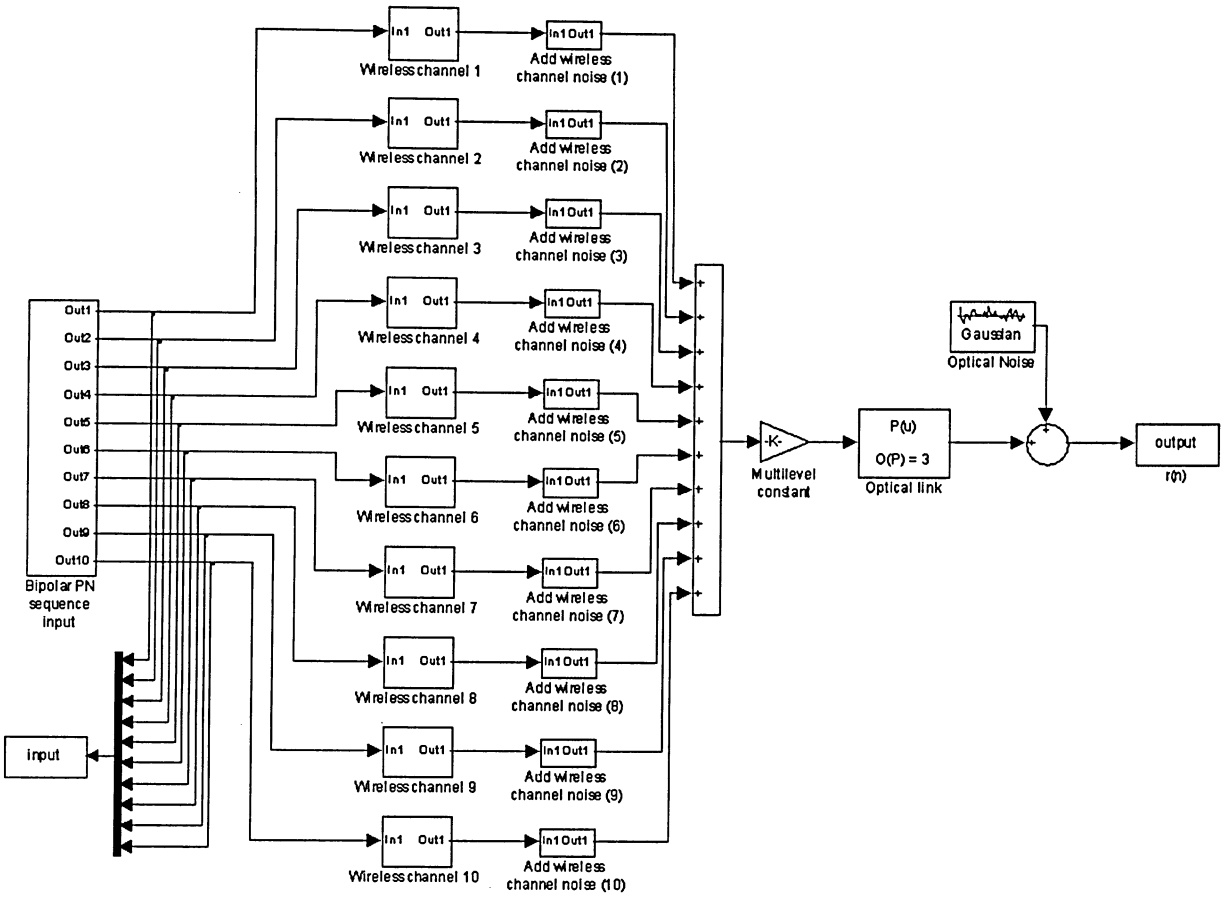

Figure 4.6: Simulink model for fiber-wireless uplink simulation.

4.7 Simulation results and discussion

We have done simulations for only multiple users with individual wireless channels. The simulation package used for all simulations herein was MATLAB with Simulink. Figure 4.6 shows the Simulink model for a multiuser CDMA environment. The Simulink model was used mainly as a means to gather the input-output data of the system. All the initializations and identification calculations (i.e. correlations) were performed in MATLAB by sending the Simulink inputs/outputs to the MATLAB workspace.

MATLAB and Simulink are the trade names of their respective owners.

4.7.1 Asynchronous communication

In the uplink it is difficult to ensure synchronous communication. This would require all transmitters to have access to a common clock [40]. Realistically, asynchronous communication takes place in the uplink and therefore, for more realistic results, all our simulations are performed in an asynchronous environment. The timing diagram of Figure 4.7 shows how the simulation is carried out. From the diagram it is clear that the input PN sequences are not synchronized. Due to the cross correlation property of PN sequences, even if different transmitters are not synchronized, the cross correlations (i.e. partial cross correlations) still hold ([41], [40]) and the algorithm is able to successfully identify both systems.

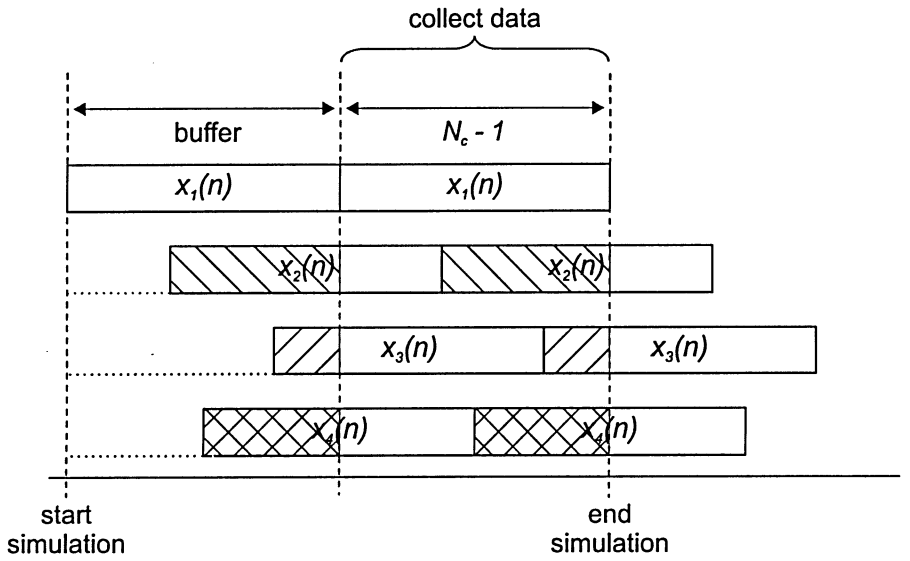

Figure 4.7: Asynchronous CDMA communication.

4.7.2 Parameters and channel characteristics

CIR: A sample of *one* of the CIRs used in the simulations is shown in Figure 4.8. All CIRs satisfied the property of unit energy, i.e. $\sum_n |h(n)|^2 = 1$. This ensured no amplification from the wireless channel.

Noise: All simulations were performed with the inclusion of additive Gaussian wireless and optical noise, $n_w(n)$ and $n_{op}(n)$, respectively. The SNR between each mobile user and the RAP was set to 25 dB, and the optical noise power was set equal to the wireless

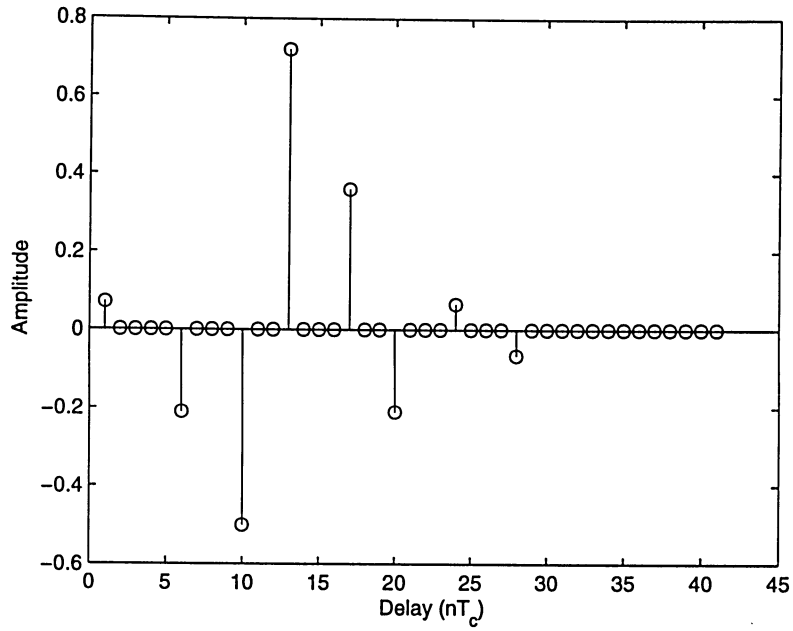

Figure 4.8: One of the CIRs used in the simulation.

noise power. There are certain environments where either the wireless channel noise or optical channel noise may be dominant [42]. However, a well designed system will have both noise of equal order.

Number of users: 10 mobile users were simulated. The effect of including additional users will also be shown.

PN sequence length: Simulations were performed with a PN sequence length of 4095 ($2^{12} - 1$). The sequence length was chosen based on various trial identifications. Acceptable results were not obtained until after a PN sequence length of 1023. At this length, the identification started to show convergence towards the actual CIR coefficients and a distinction between the actual impulse response and erroneous impulse response peaks was evident. At $N_c = 2047$ the algorithm performed well in the absence of noise, but had difficulties in the presence of noise. The PN sequence length which gave acceptable results in both the noiseless and noisy cases was $N_c = 4095$; therefore, this sequence length was used in all simulations. From this observation it can be stated that the longer the PN sequence, the better the covariance properties and hence the

better the identification. Compared to the single user case [7], identification in a multiuser environment requires a longer sequence length because there is MAI in addition to ISI.

Cross covariance: Each of the multiple PN sequences was generated from a separate maximal-length LFSR polynomial. This is in contrast to the common technique (used in current CDMA systems) of using delayed versions of a single PN sequence to represent different users. The 'delay' technique can only be used if the largest memory of the CIR is known prior to identification so that the PN sequence offset can be set larger than this value. If the PN sequence offset is not longer than the memory, there will be multiple identifications at the locations of cross covariance peaks. The ideal case would be to have zero cross covariance and perfect autocovariance within the sequence family. This would result in a perfect identification.

Quality of fit: The quality of fit of the estimated CIR to the actual CIR was measured by defining a normalized estimation error parameter

$$\rho = \frac{\sum_{k=0}^{L}[h_{actual}(k) - h_{est}(k)]^2}{L_{max}}, \tag{4.49}$$

where L_{max} is the largest CIR memory amongst all users. Dividing by L_{max} makes ρ independent of CIR memory. A smaller ρ means a better CIR estimate.

Polynomial: The major source of nonlinearity is the optical source, which can be modelled using a third order memoryless nonlinearity with a saturating characteristic. The model of the nonlinearity was discussed in Section 2.2.2.

Bit rate: The bit rate of the algorithm was calculated using the delay spread of the CIR. The delay spread was taken to be 200 ns, which is typical for an indoor environment ([43], [44]). The maximum possible CIR memory that the algorithm can handle is $L = 4095$, i.e. the memory of the channel can be as long as the PN sequence. This

translates into a chip period of

$$4095 \times T_c = 200ns$$

$$\therefore T_c = 48.84ps.$$

The theoretical maximum bit rate is then given as

$$\text{Bit rate} = \frac{1}{T_b} = \frac{1}{4095 \times T_c} = 5Mb/s.$$

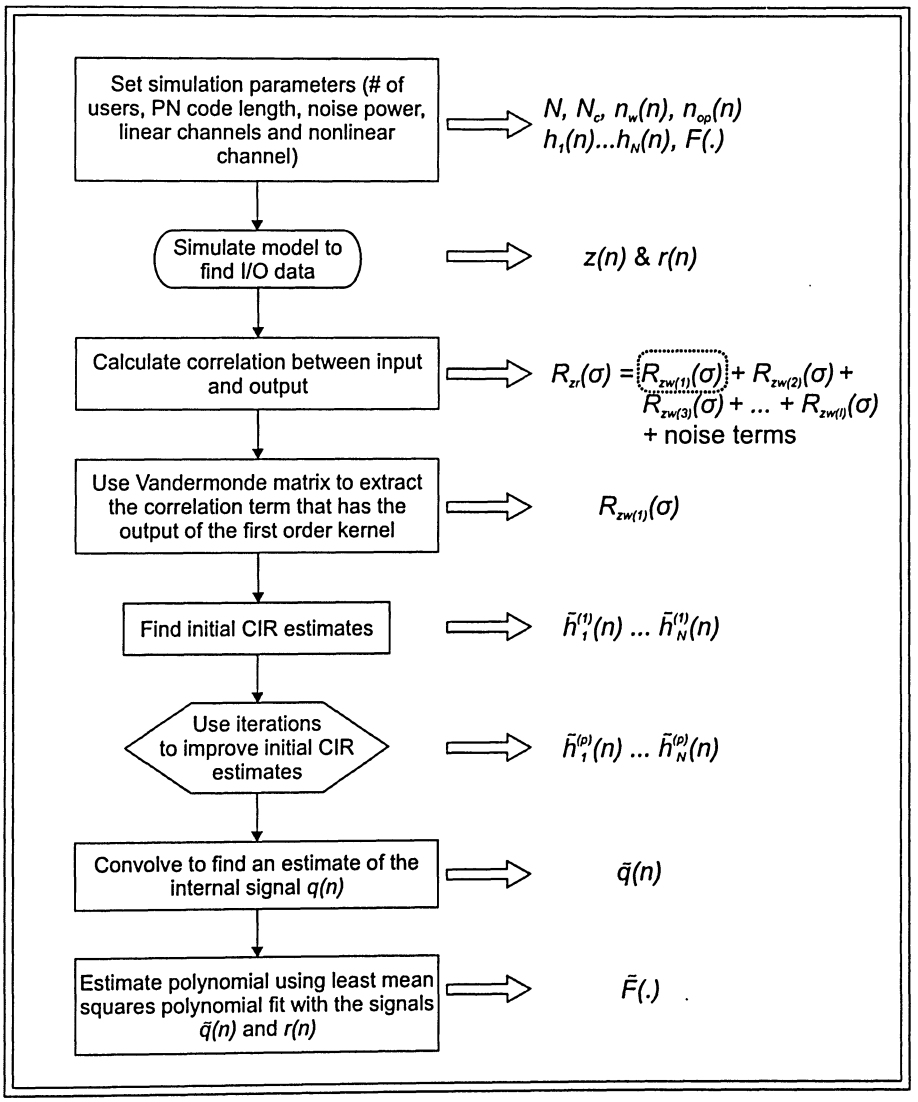

Figure 4.9: Algorithm flowchart for fiber-wireless uplink simulation.

4.7.3 Wireless channel identification

The general layout of the algorithm is shown in the flowchart of Figure 4.9. The flowchart is self-explanatory, all steps needed for identification are presented in a clear and concise manner. Since a third order nonlinearity was used, it was required to have *three* multilevel inputs when identifying the CIR; the multilevels were chosen as $\alpha = 1.0, 1.2, 1.4$. The CIR identification could have been performed just as accurately using any polynomial as long as the proper number of levels (α) was chosen (more on the restrictions of the polynomial will be discussed in Section 5.2.2).

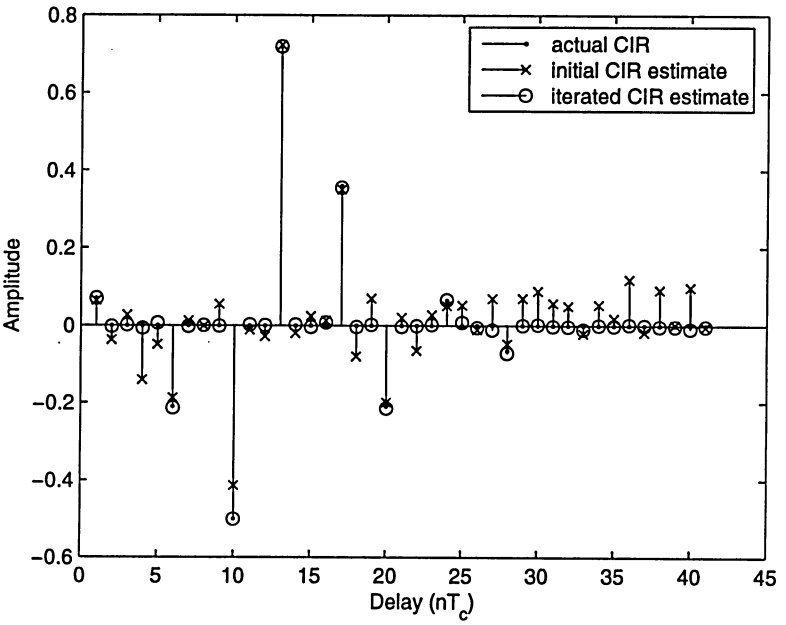

Figure 4.10: Actual, initial, and iterated CIRs ($h_1(n)$) of the wireless channel.

Figure 4.10 shows the estimated, iterated, and actual CIRs for the channel of the 1st user given by

$$h_1(n) = 0.07\delta(n) - 0.21\delta(n-5) - 0.5\delta(n-9) + 0.72\delta(n-12) + 0.36\delta(n-16) - 0.21\delta(n-19) + 0.065\delta(n-23) - 0.065\delta(n-27). \quad (4.50)$$

At first glance, it may seem that using iterations doesn't significantly improve the estimate. However, this improvement will be justified in Section 4.7.4 where it is shown that the

iterated CIR estimate translates into a much more accurate estimate of the polynomial. This is mainly due to the iterative algorithm being able to remove small non-zero erroneous peaks, but also because of a better estimate of the *actual* CIR peaks. All aspects of the identification are interconnected, so even a small improvement in the CIR estimate can go a long way in the polynomial estimate. If the initial CIR estimate is not sufficient, the iterative technique may reduce the accuracy of certain peaks, but overall the fit will still be improved.

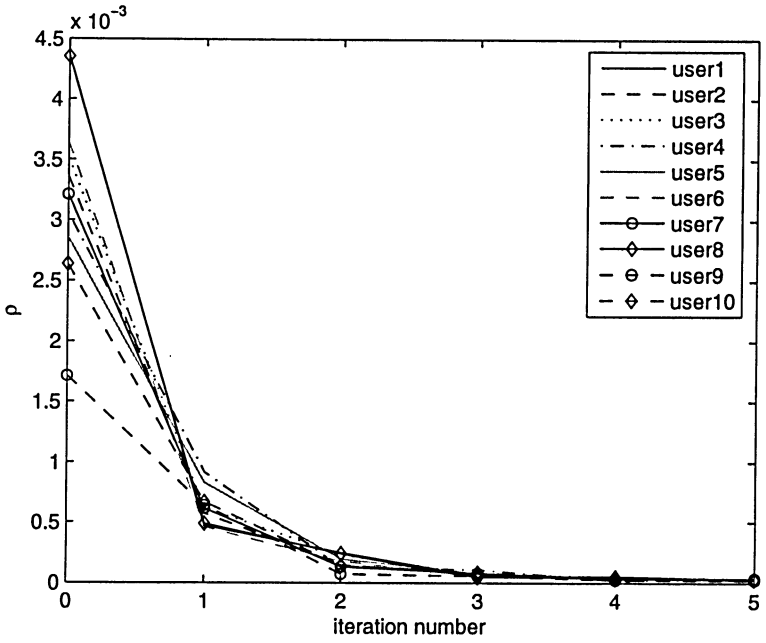

Figure 4.11: ρ versus number of iterations.

Figure 4.11 shows ρ versus the number of iterations. From this figure it is clear that after just 2 iterations there is a significant decrease in ρ. As an example, the quality of fit for user 10 improves by 94.83% over the initial CIR error, i.e. ρ improves from 2.634×10^{-3} to 0.1361×10^{-3}. Further iterations (> 3) result in little change in the quality of fit. Nevertheless, an accurate CIR estimate is a strict requirement for the nonlinear estimation, so the number of iterations used in all subsequent simulations is 5, unless otherwise specified. Another observation from Figure 4.11 is that initially, at 0 iterations, each user has a different value for ρ. This is due to the characteristics of that users CIR (the delay between multipath arrivals and the peak amplitudes). Although initially each user has a different value for ρ, a

common value is reached after the iterations are performed.

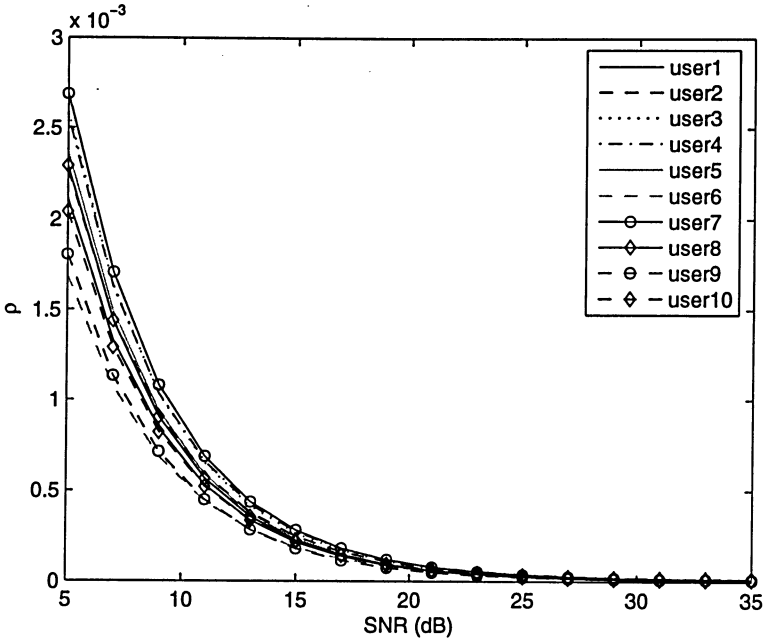

Figure 4.12: Final ρ (after 5 iterations) versus SNR.

The final ρ (after 5 iterations) versus SNR is shown in Figure 4.12. Even though theoretically the noise is not correlated with the signal, ρ starts to increase rapidly for SNR $\leq$ 20 dB. This presents a practical limitation; the algorithm requires an SNR $>$ 20 dB in order to give an acceptable identification. After $\sim$25 dB, the improvement resulting from iterations is minimal. Therefore, an SNR of 25 dB was used in all simulations.

Figure 4.13 shows ρ versus the number of iterations at an SNR of 15 dB. This figure is included to show the effect of a hostile noise environment. In this case, even using iterations will not cause the error to converge close to zero. ρ converges at a noise floor of approximately 2.445×10^{-4} after 5 iterations. The noise floor increases with decreasing SNR.

4.7.4 Fiber link identification

As mentioned above, the estimate of the polynomial is directly dependent on the quality of the estimate of the wireless channel. Essentially, the validity of the CIR estimate can be verified by observing how close of a polynomial estimate it produces. Even the slightest

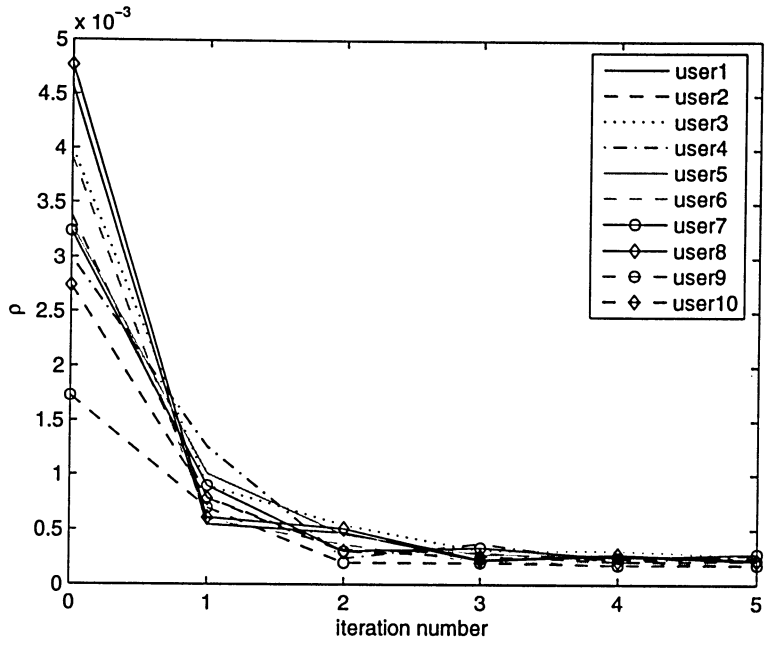

Figure 4.13: ρ versus number of iterations with SNR = 15 dB.

errors in the CIR estimate can be detrimental when estimating the internal signal $q(n)$.

The nonlinear channel used in the simulations was a 3rd order saturating memoryless nonlinearity given by the polynomial

$$r(n) = -0.35q^3(n) + q(n). \tag{4.51}$$

It is important to state that the nonlinear system **must** have a linear coefficient A_1, otherwise identification of neither the linear channels nor nonlinear channel is possible. Without the A_1 coefficient, the equations relating the cross covariance to the CIR (equations (4.34) & (4.43)) would become zero.

The fit of the nonlinear identification depends on how much data is available, and so it is desired to have the input cover a large dynamic range. A PN sequence length of 4095 and the multipath conditions of the linear channels ensured that a large dynamic range was available for the polynomial fit.

Figures 4.14(a) and 4.14(b) show the estimated polynomial (with and without using iterations) for an SNR of 25 dB and 15 dB, respectively. When using iterations there is a significant increase in the accuracy of the polynomial estimates. For an SNR of 25 dB the

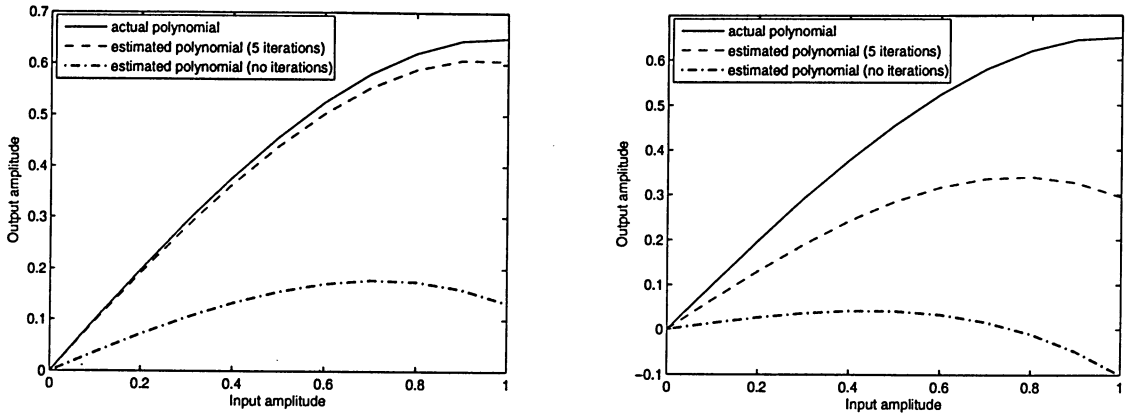

(a) Estimated nonlinearity of the fiber link using an SNR of 25 dB.

(b) Estimated nonlinearity of the fiber link using an SNR of 15 dB.

Figure 4.14: Comparison of polynomial estimates (with and without using iterations).

estimated polynomial (using iterations) was

$$r(n) = -0.3559q^3(n) - 0.0095q^2(n) + 0.9716q(n), \tag{4.52}$$

which is accurate when compared to the actual polynomial of equation (4.51). The MSE for the above case was 5.5954×10^{-4}. This estimate is obviously quite good, however, the accuracy of the identification deteriorates with decreasing SNR. For an SNR of 15 dB, the estimated polynomial (using iterations) was

$$r(n) = -0.3505q^3(n) - 0.0241q^2(n) + 0.6693q(n), \tag{4.53}$$

which has an MSE of 4.288×10^{-2}. This again shows the practical limitation of the algorithm.

4.7.5 Additional users

The effect of additional users is shown in Figures 4.15 and 4.16. With additional users it takes more iterations to decrease ρ and the estimated polynomial starts to move further away from the actual one. On average, $\rho = 1.212 \times 10^{-4}$ with 18 users and 10 iterations but $\rho = 3.012 \times 10^{-5}$ with 10 users and 5 iterations. Even after 10 iterations the algorithm with 18 users is unable to come close to the algorithm with 10 users. The difference between the two ρ's is due to residual MAI.

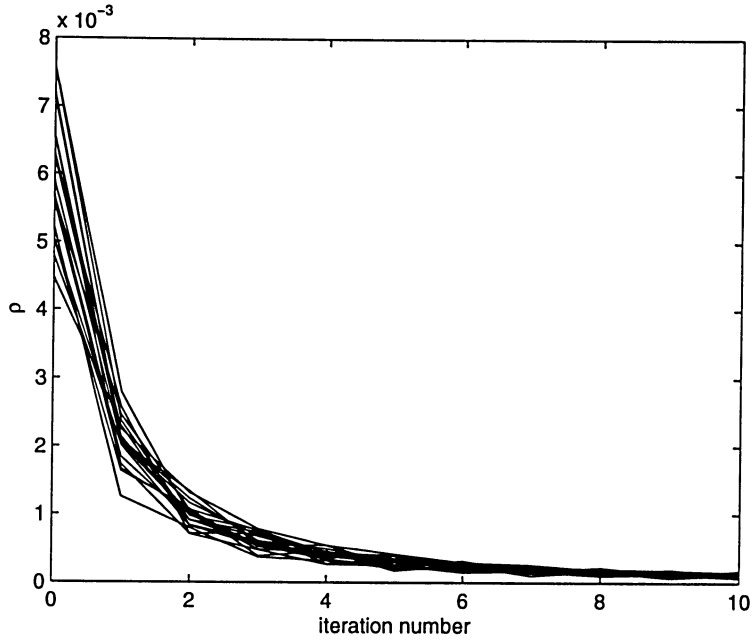

Figure 4.15: ρ versus number of iterations for 18 users (each line corresponds to one user).

With 18 users the iterative algorithm still improves the CIR estimate and removes MAI, but the requirements on the *initial* CIR estimate start causing a noticeable error in the polynomial estimate. As the number of users increases past 18, the identification starts to degrade rapidly. This is because our iterative algorithm is unable to cope with the additional MAI. This problem can be solved by increasing the PN sequence length, however this is not a practical solution. Future work calls for investigating this scenario.

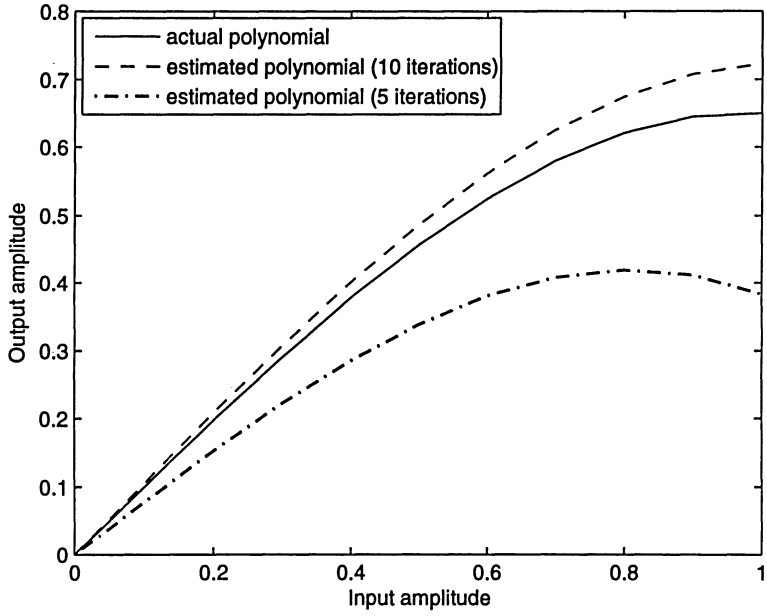

Figure 4.16: Estimated nonlinearity with 18 users.

Chapter 5

Fiber-wireless uplink equalization

Having estimated the fiber-wireless uplink in Chapter 4, equalization can now be applied to the wireless channel and nonlinear compensation to the optical link. The linear and nonlinear parts are compensated for individually, allowing for a modular architecture that is desirable for commercial implementation. The structure of the fiber-wireless equalizer is shown in Figure 5.1. The receiver consists of a polynomial, which inverse models the optical link, followed by a linear DFE arrangement that compensates for the wireless channel dispersion. The validity of the estimation algorithm is tested by error rate analysis via the said equalization and compensation techniques.

5.1 Wireless channel equalization by DFE

Decision feedback equalizers have been successfully used in equalizing wireless communication channels (refer to [45] and the references therein). DFEs have good performance at moderate complexity, work well in equalizing frequency selective fading channels, and the equalization taps can be obtained directly from the channel estimate; this is a major benefit in our case. It is shown in [22] that a DFE is superior to a linear equalizer. A considerable performance gain comes from including the feedback portion. In addition, some work in using a DFE in a fiber-wireless channel has already been done in [15]. For the reasons presented above, a DFE is implemented for equalization of the *wireless channel* of the fiber-wireless uplink in this thesis. The architecture of a DFE is shown in Figure 5.1. It consists of 2 linear transversal filters, a decision device, and a feedback loop. The DFE is classified

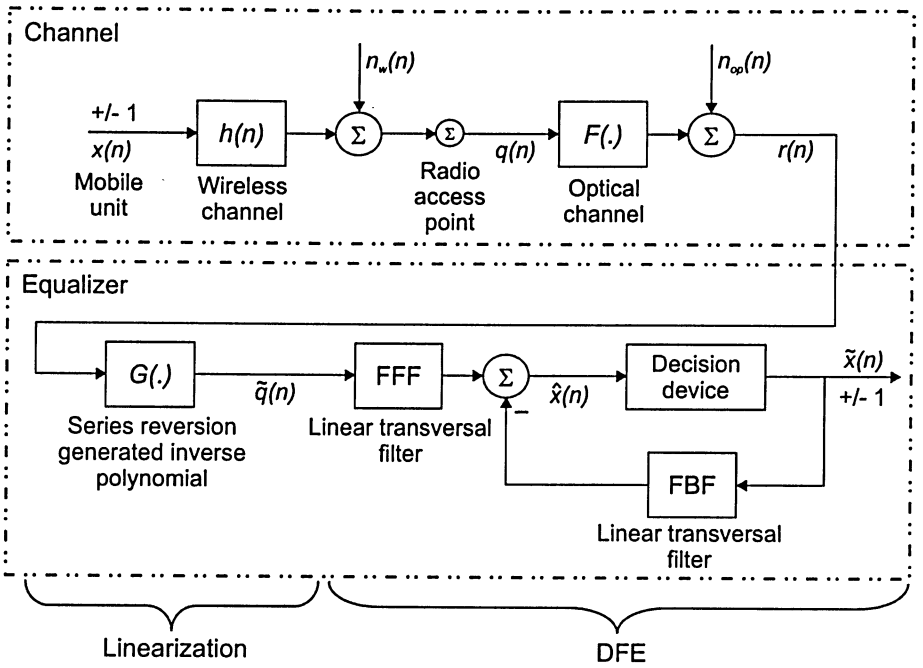

Figure 5.1: Block diagram for fiber-wireless uplink equalization.

as a nonlinear equalizer, where the nonlinearity can be attributed to the decision device. A stand alone DFE is most efficient in equalizing linear channels.

The goal in a DFE system is to determine the current input, and then calculate and remove all ISI that the current input contributes to subsequently received inputs. The feed forward filter (FFF) in Figure 5.1 is used to eliminate the contribution from the precursors of the wireless channel, and the feedback filter (FBF) in Figure 5.1 is used to eliminate that part of the ISI from the present estimate caused by previously detected symbols. The linear filter coefficients are optimized in order to maximally equalize the ISI. The MSE criterion is used for optimization of the equalizer coefficients. Optimization of the DFE coefficients is a well established technique when the CIR is known [22]. So the FFF and FBF taps can be readily determined once the CIR has been estimated.

The output of the DFE in Figure 5.1 can be expressed as

$$\hat{x}(k) = \sum_{j=-K_1}^{0} c_j \tilde{q}(k-j) + \sum_{j=1}^{K_2} c_j \tilde{x}(k-j), \tag{5.1}$$

where c_j are the tap coefficients, and the equalizer has $(K_1 + 1)$ feedforward taps and K_2

feedback taps. The MSE criterion for optimization yields

$$J(K_1, K_2) = E|x(k) - \hat{x}(k)|^2, \tag{5.2}$$

which can be used to determine the FFF taps using the following equation[1]

$$\sum_{j=-K_1}^{0} \psi_{lj} c_j = \tilde{h}_1^{(p)}(-l), \tag{5.3}$$

where $l = -K_1, ..., -1, 0$. The terms ψ_{lj} are defined as

$$\psi_{lj} = \sum_{m=0}^{-l} \tilde{h}_1^{(p)}(m)\tilde{h}_1^{(p)}(m + l - j) + N_0\delta_{lj}, \tag{5.4}$$

where N_0 is the equivalent noise variance of all noise sources and $l, j = -K_1, ..., -1, 0$. The FBF taps can be found from the FFF taps using

$$c_k = \sum_{j=-K_1}^{0} c_j \tilde{h}_1^{(p)}(k - j), \tag{5.5}$$

where $k = 1, 2, ..., K_2$. A drawback of DFEs is that incorrect decisions can propagate through the feedback loop and enhance, rather than remove, ISI. Incorrect decisions can also cause errors in subsequent decisions as well. However, as SNR increases, the chance of error propagation decreases. The performance loss due to incorrect decisions being fed back is approximately 2 dB [22]. This value may change depending on the CIR.

5.2 Optical channel compensation

Related work on nonlinear compensation is presented below before introducing the series reversion approach which was used for compensation in this thesis.

5.2.1 Related work on nonlinear compensation

Several approaches have been proposed to characterize and solve the problem of nonlinear distortion. In [46], the authors demonstrated how external light injection into a directly

[1]Note: the subscripts used in the DFE equations are not related to the subscripts used for the estimation derivations, except for p. They are simply used for continuity with [22].

modulated laser diode can be used to enhance the linear performance of an ROF system. This is done by making the modulation response of the device more linear around the RF band of operation. In [47], low-cost predistortion circuits able to compensate second- and third-order laser distortions in multiservice ROF industrial systems were developed. Other approaches attempt to use a post nonlinearity recovery block by means of solving the laser rate equations [13]. In the above approaches, knowledge of the device parameters is needed because they use either additional hardware or require the solving of laser rate equations. The drawback here is that device parameters can be device dependent or sometimes not even available, and can even vary amongst similar devices. Instead of focusing on compensation at the electronics level or by using the rate equations, this thesis focuses on a higher level systems approach. Here, the nonlinearity is looked at in terms of its input-output characteristics, and then compensated for accordingly. An advantage of the systems approach is that additional nonlinearities can be modelled as well, i.e. those from amplifiers. This approach is similar to adaptive asymmetric linearization reported in [10].

5.2.2 Linearization by series reversion

Nonlinear channel compensation is implemented in this thesis by including an inverse polynomial (or additional filter) prior to the aforementioned DFE. This results in an architecture called the Hammerstein type DFE [15]. The fiber-wireless uplink is a Wiener system and so a Hammerstein type equalizer would be the natural choice for a block-oriented compensation scheme. A Hammerstein type DFE was developed for a Wiener system for a single user environment in [15]. In this thesis, equalization is still done in a single user environment, but using the estimated parameters from the MU case.

The additional filter in this thesis is generated using series reversion. The idea is to determine how well the developed identification algorithm performs, and series reversion provides a sufficient indication of this. Series reversion is one of the simplest techniques for nonlinear compensation and therefore has its limitations. A comprehensive treatment on series reversion is given by Tsimbinos in [48]. Some advantages of series reversion include: 1) simplicity, 2) once $F(.)$ is known, finding the coefficients of $G(.)$ is straightforward, 3) no need

for adaptive methods as in [10], 4) low complexity is attractive for practical implementation, and 5) simple yet effective for the fiber-wireless uplink. Some disadvantages include: 1) limited amplitude interval for inversion; beyond this interval the system produces increasing distortion and overpowers the inversion, and 2) dependence on nonlinearity strength. It is important to mention that series reversion works well in inverting a weak nonlinearity with a saturating characteristic; in this case, series reversion provides a significant CER improvement that will be shown in Section 5.3. More elaborate nonlinearities will require different compensation techniques.

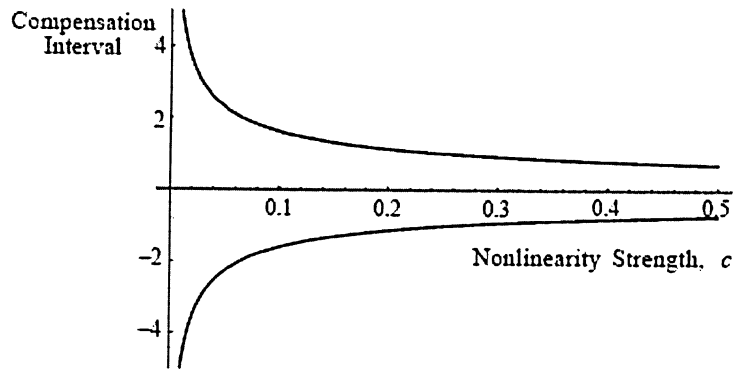

Figure 5.2: Compensation interval versus strength of 3rd order nonlinearity [48].

One of the major issues with series reversion is the limited compensation interval due to nonlinearity strength. The compensation interval for different values of nonlinearity strength, c, are shown in Figure 5.2 for the polynomial $y = cx^3 + x$. Conveniently, the polynomial considered above has the same structure as the polynomial considered in the simulations of the fiber-wireless uplink, i.e. $r(n) = -0.35q^3(n) + q(n)$. From Figure 5.2 it is clear that as the strength of the nonlinearity increases, the compensation interval decreases. However, series reversion is still sufficient because only weak saturating nonlinearities are relevant in the optical link, and the nonlinear compensation is performed on normalized inputs.

The polynomial $F[.]$ and the inverse polynomial $G[.]$ are defined as

$$r(n) = F[q(n)] + n_{op}(n) = A_1 q(n) + A_2 q^2(n) + ... + A_l q^l(n) + n_{op}(n), \qquad (5.6)$$

and

$$\tilde{q}(n) = G[r(n)] = g_1 r(n) + g_2 r^2(n) + g_3 r^3(n) + ... + g_{l_{inv}} r^{l_{inv}}(n), \tag{5.7}$$

respectively, where l is the order of the polynomial and l_{inv} is the order of the inverse polynomial. The series reversion generated coefficients of the inverse polynomial $G[.]$ are given in terms of A_k as

$$g_1 = \frac{1}{A_1}, \quad g_2 = -\frac{A_2}{(A_1)^3}, \quad g_3 = \frac{2(A_2)^2 - A_1 A_3}{(A_1)^5}, \quad g_4 = \frac{5A_1 A_2 A_3 - A_4 (A_1)^2 - 5(A_2)^3}{(A_1)^7} \tag{5.8}$$

$$g_5 = \frac{6A_2 A_4 (A_1)^2 + 3(A_1)^2 A_3^2 + 14(A_2)^4 - A_5 (A_1)^3 - 21 A_1 A_3 (A_2)^2}{(A_1)^9}, \quad g_6 = ..., \quad g_7 = ..., \tag{5.9}$$

where g_6 and g_7 can be found in [49]. The order of the inverse polynomial l_{inv} must be selected to maximize linearity. The resulting compensation contains higher order nonlinear terms that produce distortion which is negligible at low signal amplitudes but become detrimental at high signal amplitudes [48]. This affects the compensation interval.

5.3 Simulation results and discussion

The channel is estimated under a multiuser environment, but the equalization is done only for a single user. The simulation parameters were the same as in Section 4.7.2. Additional parameter definitions include the order of the inverse polynomial $G[.]$, and the number of DFE taps. A 7^{th} order polynomial was selected for the inverse by testing the linearity of the combined system $F[.]$ and $G[.]$ under various orders. A 7^{th} order inverse resulted in the most linearized output. The number of DFE taps were derived based on the memory of the CIR from Figure 4.8, which has a memory of $L = 28$. In order to completely eliminate post-cursor interference, the number of FBF taps must satisfy the condition $K_2 \geq L$ [22]. The number of FFF taps is chosen to be approximately $2L$, which is common in the literature. So, the DFE parameters for the simulation were 56 FFF taps and 28 FBF taps.

Figure 5.3 shows the CER performance of the estimation algorithm for 2 different cases: 'MU estimation' (with details specified on the figure) and 'Single user estimation.' 'MU estimation' refers to the scenario where the equalization and compensation parameters are

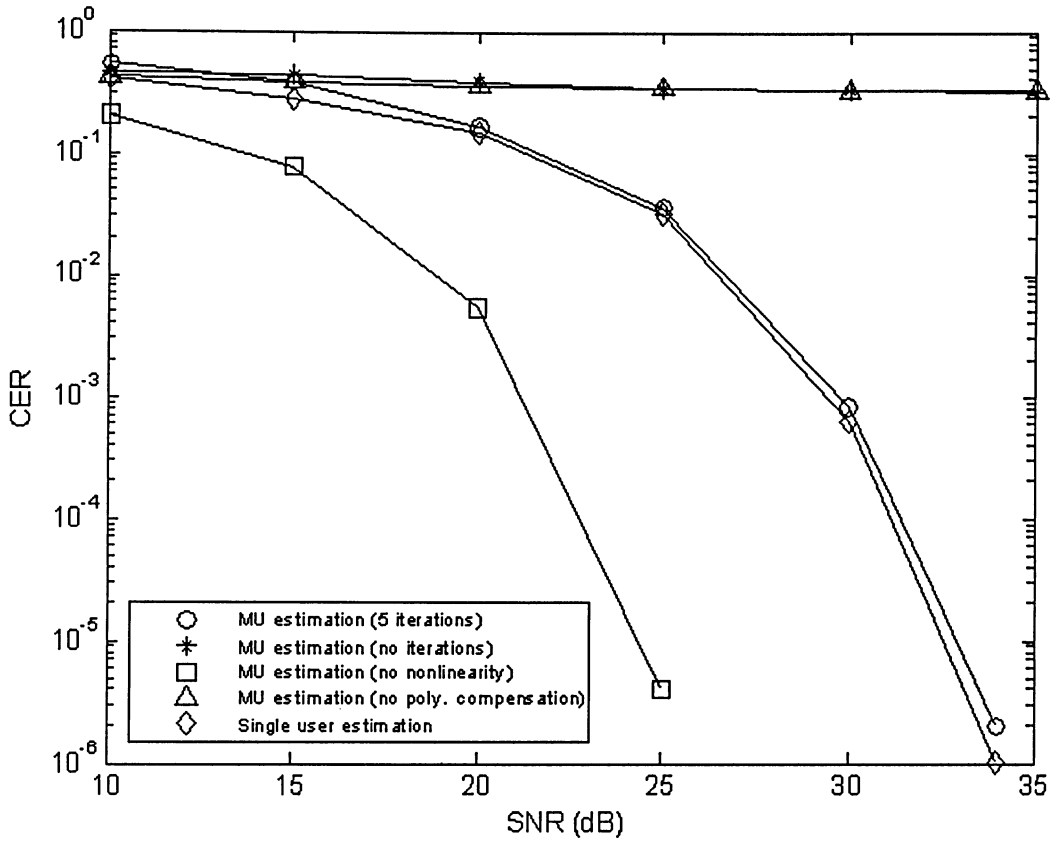

Figure 5.3: CER of fiber-wireless uplink.

derived using the channel characteristics found from MU estimation (the ones from Section 4.7). 'Single user estimation' refers to the scenario where the equalization and compensation parameters are derived using the channel characteristics found from single user estimation.

It is important to mention that CER is much larger than BER. A correct decision on a bit can still be made in the presence of many chip errors. For example, it was shown by Cypher *et al.* [50] that, when using 64 chips to represent 1 bit, the BER lags behind the CER by 18 dB. As a rough estimate, take the SNR lag between the BER and CER to be 20 dB (in our case N_c is large so we have a lag greater than 18 dB).[2] An acceptable BER for transmitting data is 10^{-6}. Taking into consideration the BER approximation above, our algorithm can achieve this BER at an SNR of about 15 dB, which is comparable to the DFE

[2]Further mathematical analysis is needed in order to find the exact CER to BER conversion factor.

BER curves obtained in [15] and [22].

Some important conclusions from Figure 5.3 are:

1. Correlation analysis alone gives unacceptable CER. The trace marked by $*$'s remains high even as SNR increases.

2. Supplementing correlation analysis with the iterative algorithm results in an improvement over the non-iterated CER. This is shown by the traces marked by $\circ$'s and $*$'s. For an SNR > 15 dB, the CER marked by $\circ$'s starts to improve, whereas the $*$ trace remains high.

3. The iterative algorithm works well in removing MAI. This can be seen by examining the traces marked by $\circ$'s and $\diamond$'s. These two CERs are adjacent to one another, meaning that with the iterative algorithm, the performance of MU estimation comes close to that of single user estimation. The $\circ$ trace has a slightly worse CER than the $\diamond$ trace. This can be attributed to residual MAI.

4. Without polynomial compensation the CER is unacceptable ($\triangle$). The performance in this case is highly undesirable. The CER remains high, irrespective of high SNR, because the DFE alone is unable to compensate for the nonlinearity. This justifies the use of series reversion for polynomial compensation.

5. The trace marked by $\square$'s is the performance of the DFE in a linear channel. Better polynomial compensation methods will shift the CER ($\circ$) to the left, i.e. towards the $\square$ trace. However, this will require more complex polynomial compensation techniques than series reversion. For example, series reversion can be improved by using orthogonal polynomials and orthogonal inverses to overcome some of the negative effects of residual terms [48].

It should also be mentioned that CER performance depends greatly on the CIRs severity of multipath conditions. This is shown in [22], where the error rate performance of various CIRs is compared to a channel with no ISI. The performance can vary significantly depending on the CIR.

Chapter 6

Fiber-wireless downlink estimation using Walsh codes

This chapter presents an investigation into the estimation of the *wireless channel* of the fiber-wireless downlink in a multiuser CDMA environment using Walsh codes. An investigation into the single signal estimation of a Hammerstein system has been covered in [34], but Gaussian input were used and there was no extraction of the term $\Re_{zw_1}(\sigma)$. In this chapter, the theory is extended to the multiuser case where varying wireless channels are encountered for each mobile user, and it is also shown that multilevel testing (via the Vandermonde matrix) works in the downlink as well.

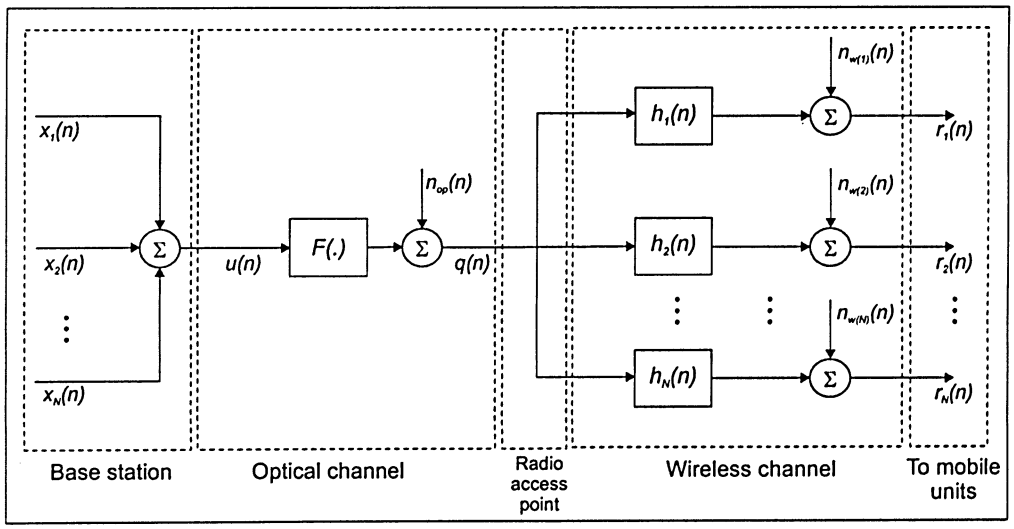

Figure 6.1: Fiber-wireless downlink in a multiuser CDMA environment.

The block diagram in Figure 6.1 shows the fiber-wireless downlink in a multiuser CDMA

Symbol	Description
$x_j(n)$	input Walsh code spreading sequence, $1 \leq j \leq N$
$u(n)$	compound Walsh signal input
$F(\cdot)$	optical channel nonlinear function
$n_{op}(n)$	optical receiver Gaussian noise
$q(n)$	signal sent through multiple wireless channels
$h_j(n)$	wireless channel impulse response, $1 \leq j \leq N$
$n_{w(j)}(n)$	wireless channel Gaussian noise, $1 \leq j \leq N$
$r_j(n)$	signal sent to mobile units, $1 \leq j \leq N$

Table 6.1: Symbol descriptions for fiber-wireless downlink.

environment. All signals used in analyzing the fiber-wireless downlink, along with their descriptions, are shown in Table 6.1. The channel of interest will be that of the first user, and therefore the output signal used in all following derivations will be $r_1(n)$. Proceeding to the estimation theory, the output of the nonlinear system plus the optical noise is given by a polynomial of the form

$$q(n) = A_1 u(n) + A_2 u^2(n) + ... + A_l u^l(n) + n_{op}(n), \tag{6.1}$$

where $u(n)$ is a compound input of Walsh codes (of length N_w) that can be written as

$$u(n) = x_1(n) + x_2(n) + ... + x_N(n). \tag{6.2}$$

The downlink estimation is similar to the MUc estimation when considering only one wireless branch in Figure 6.1. The major difference being that the two channels are reversed. The system output $r_1(n)$ can be expressed by the convolution

$$r_1(n) = q(n) * h_1(n) + n_{w(1)}(n). \tag{6.3}$$

Substituting for $q(n)$ and expanding the convolution gives

$$r_1(n) = A_1 \sum_{m=-\infty}^{\infty} h_1(m)u(n-m) + A_2 \sum_{m=-\infty}^{\infty} h_1(m)u^2(n-m) \tag{6.4}$$

$$+ ... + A_l \sum_{m=-\infty}^{\infty} h_1(m)u^l(n-m) + \sum_{m=-\infty}^{\infty} h_1(m)n_{op}(n-m) + n_{w(1)}(n), \tag{6.5}$$

which can be written in a more compact form as

$$r_1(n) = \sum_{k=1}^{l} \left(A_k \sum_{m=-\infty}^{\infty} h_1(m) \prod_{i=1}^{k} u(n-m) \right) + \underbrace{\sum_{m=-\infty}^{\infty} h_1(m) n_{op}(n-m) + n_{w(1)}(n)}_{\text{noise terms}}. \quad (6.6)$$

As a summation of the output of the isolated l^{th} order kernel, the above equation becomes

$$r(n) = w_1(n) + w_2(n) + w_3(n) + ... + w_l(n) + \text{noise terms}. \quad (6.7)$$

In the downlink, multilevel testing is implemented prior to the optical channel by using the signal $\alpha_m u(n)$, where $\alpha_m \neq \alpha_l \ \forall \ m \neq l$, and repeating l times. Given that the output can be expressed by equation (6.7), it can easily be shown using the same procedure as in Section 4.5.1 that multilevel inputs can be used to extract $\Re_{uw_1}$ from $\Re_{ur}$. Therefore, the input-output correlation can be written as

$$\boxed{\Re_{ur_{\alpha_m}}(\sigma) = \sum_{k=1}^{l} \alpha_m^k \Re_{uw_k}(\sigma), \quad m = 1, 2, ..., l}, \quad (6.8)$$

giving the same relationship as in equation (4.25).

6.1 Difficulties with the input-kernel correlation

The cross covariance between the compound input $u(n)$ and $w_1(n)$ can be written as

$$\Re_{uw_1}(\sigma) = \overline{w_1(n)u(n-\sigma)}. \quad (6.9)$$

Substituting for $w_1(n)$ and expanding $u(n)$ gives

$$\begin{aligned} \Re_{uw_1}(\sigma) &= \overline{\left(A_1 \sum_{m=-\infty}^{\infty} h_1(m)u(n-m) \right) \left(u(n-\sigma) \right)} \\ &= A_1 \sum_{m=-\infty}^{\infty} h_1(m) \overline{u(n-m)u(n-\sigma)} \quad (6.10) \\ &= A_1 \sum_{m=-\infty}^{\infty} h_1(m) \overline{(x_1(n-m) + x_2(n-m) + ... + x_N(n-m))} \\ &\qquad \overline{(x_1(n-\sigma) + x_2(n-\sigma) + ... + x_N(n-\sigma))}. \quad (6.11) \end{aligned}$$

The above equation can be considered two ways: 1) by expanding $u(n)$, giving equation (6.11), and 2) without expanding $u(n)$, giving equation (6.10).

1) Expanding $u(n)$

Simplifying equation (6.11) using correlation notation gives

$$\Re_{uw_1}(\sigma) = A_1 \sum_{m=-\infty}^{\infty} h_1(m)\big(\Re_{x_1x_1}(m-\sigma) + \Re_{x_2x_2}(m-\sigma) + ... + \Re_{x_Nx_N}(m-\sigma) + \Re_{x_ix_{j(j\neq i)}}(m-\sigma)\big). \quad (6.12)$$

Since Walsh codes do not have well defined mathematical correlation properties as PN sequences, the above equation cannot be further simplified. Individually, Walsh codes only have good correlation properties when tightly synchronized and even then, it is only at the zeroth lag. As the lag moves away from zero the correlation becomes unacceptable. This is represented in Figure 6.2. This figure shows the autocovariance and cross covariance properties of two individual Walsh codes, one with a code index of 396 and the other with a code index of 882. From Figures 6.2(a) and 6.2(b) it is clear that the autocovariance properties of individual Walsh codes is unacceptable. For this reason, identification of the concatenated channel in a single user Walsh code environment is difficult. But the situation drastically changes when many users are considered at once.

2) Without expanding $u(n)$

The covariance properties of the *summation* of Walsh codes is very much different from the covariance of individual Walsh codes. It has been found through simulations that, as more and more users are added, this compound input of Walsh codes starts to resemble a white noise-like process. This is an interesting outcome because it is known that identification of the fiber-wireless downlink is possible under the condition that the input is white noise-like ([34], [8]). The autocovariance of the input $u(n)$ is shown in Figure 6.3. There is some resemblance observed between this autocovariance and that of the PN sequence, given by $\Re_{x_ix_i}(\lambda) = N_c\delta_i(\lambda)$. Aside from the amplitudes at non-zero lags, the autocovariance of the summation of Walsh codes can be approximated by the relationship[1]

$$\Re_{uu}(\lambda) \approx N_w N\delta(\lambda), \quad (6.13)$$

[1]Under the condition that the code indices for the Walsh codes occupy the entire range of indices available for that certain code length, in equal intervals.

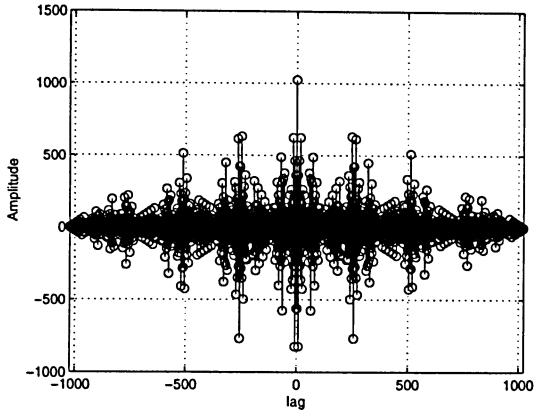

(a) Autocovariance of Walsh code of index 396.

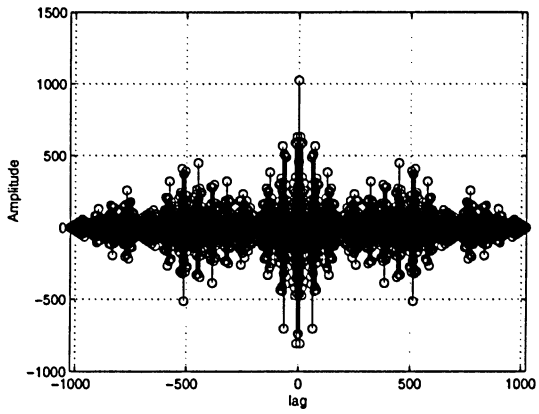

(b) Autocovariance of Walsh code of index 882.

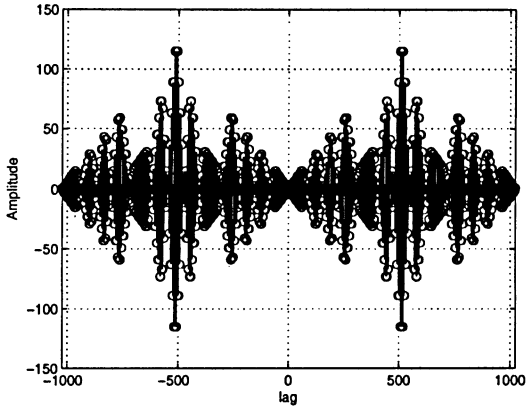

(c) Cross covariance of above two Walsh codes.

Figure 6.2: Covariance properties of individual Walsh codes of length 2^{10} for two different code indices.

where N is the number of Walsh codes. Applying the above approximation to equation (6.10) gives

$$\Re_{uw_1}(\sigma) = A_1 N_w N \sum_{m=0}^{N_w-1} h_1(m)\delta(m-\sigma). \tag{6.14}$$

Using the convolution properties of the impulse function gives

$$\boxed{\Re_{uw_1}(\sigma) = A_1 N_w N h_1(\sigma)}, \tag{6.15}$$

which is exactly the same as the covariance for the MUc case in equation (4.34). Therefore, it has been shown that the CIR can be estimated by utilizing the autocovariance property of summed Walsh codes. Using a greater number of Walsh codes results in even better

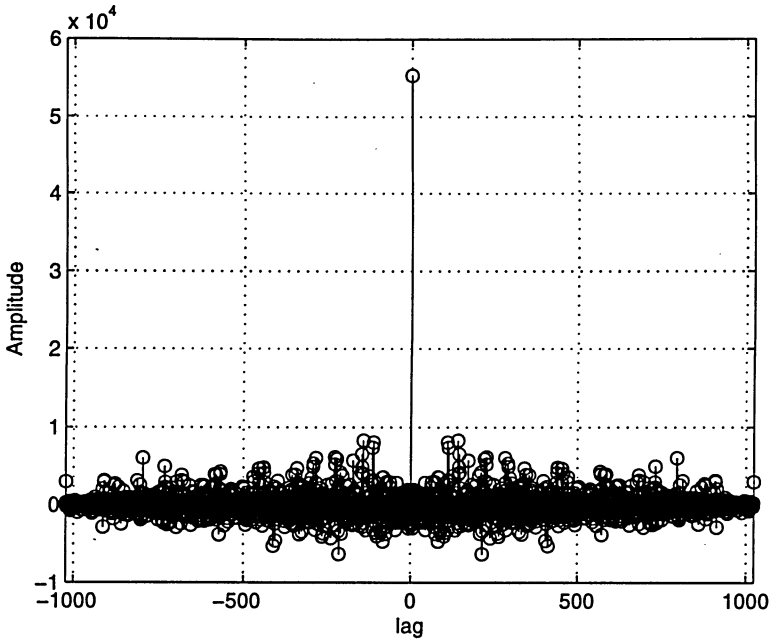

Figure 6.3: Autocovariance of a summation of Walsh codes.

covariance properties and hence a more accurate identification.

6.2 Simulation results and discussion

Figure 6.4 shows the simulation model for the fiber-wireless downlink. Parameters and channel characteristics are described below.

CIRs and polynomial: Refer to Section 4.7.2.

Noise: The SNR between the base station and RAP was set to 25 dB, and the wireless noise power for each mobile user was set equal to the optical noise power.

Number of users: 54 users were simulated at the base station.

Walsh code length: Simulations were performed with a Walsh code length of 1024 (2^{10}).

Cross covariance: Lang *et al.* showed in [29] that, for 10^{th} degree sequences, the average Walsh code cross covariances are approximately 2.53 times larger than PN sequence cross covariances. However, the adverse effect of these cross covariances are minimal

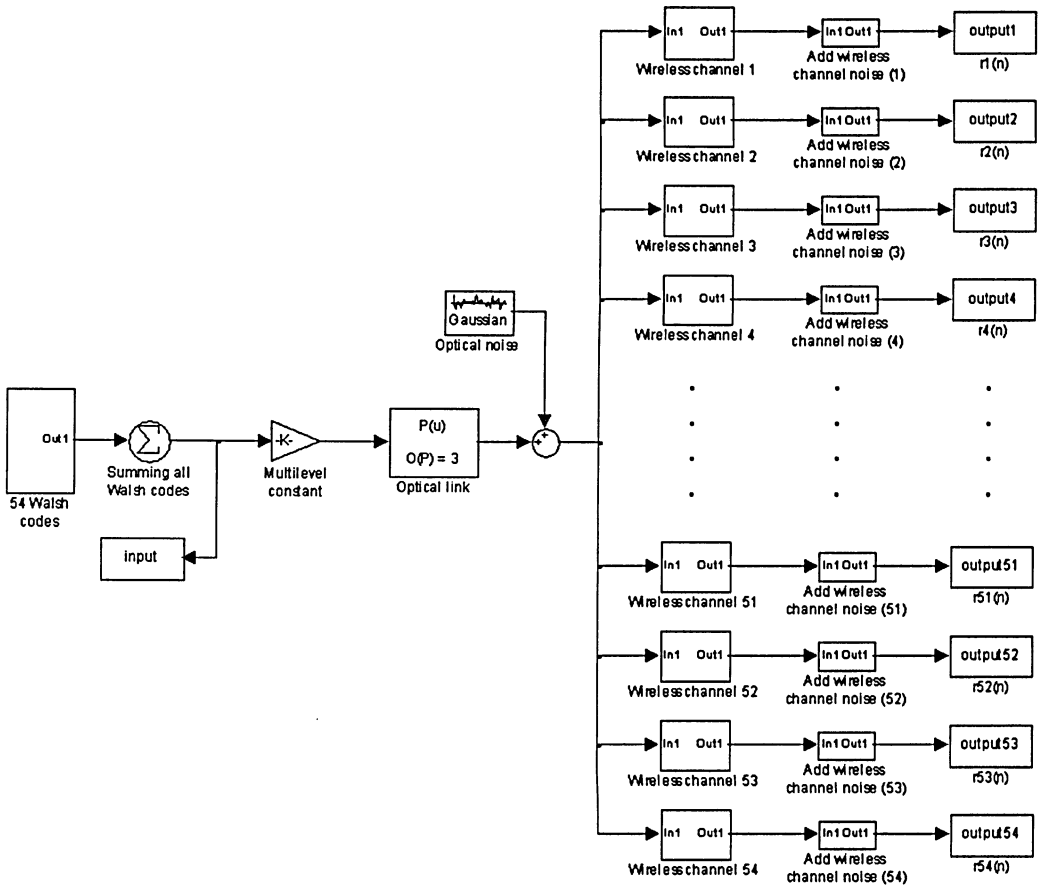

Figure 6.4: Simulink model for fiber-wireless downlink simulation.

because they are relatively small when compared to the large autocovariance value. This can also be seen by comparing Figures 6.2(c) and 6.3. From these figures it is found that the maximum amplitude of the cross covariance is approximately 0.208% of the maximum autocovariance.

Quality of fit: Refer to Section 4.7.2.

Synchronous communication: Synchronization can be achieved for all signals in the fiber-wireless downlink. The buffer period needed for the simulation of asynchronous communication is not needed. All signals can start at the same time and data is collected from the start of the simulation to the end (i.e. the time needed to cover one period, N_w).

6.2.1 Wireless channel identification

Two CIR estimates are presented in this section, they are defined as 'good' and 'poor'. The reason for this is to show that at this point there is an inconsistency between estimates and that the quality of the estimate depends on the characteristics of the CIR (a major factor being the spread between multipath arrivals). Figures 6.5 and 6.6 show the estimated and actual CIR for the two different channels. There is a greater spread between multipath arrivals in the 'poor' estimate of Figure 6.5; therefore, the algorithm is not as accurate but it is still able to recover the general structure of the desired CIR.

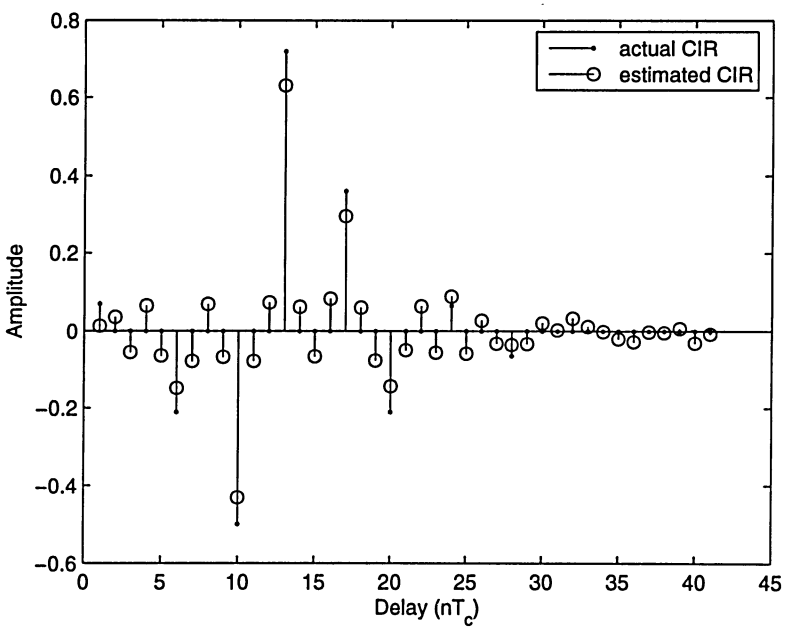

Figure 6.5: 'Poor' CIR estimate.

The quality of the CIR estimate, ρ, can be compared with the MU estimation of Section 4.7.3. Figure 6.5 has $\rho = 4.241 \times 10^{-3}$ and Figure 6.6 has $\rho = 1.462 \times 10^{-4}$. When comparing to Figure 4.11, the 'poor' estimate is comparable to doing no iterations and the 'good' estimate is comparable to doing 2 iterations. Contrarily to MU estimation, for Walsh code estimation there is a large difference amongst users ρ's. The significance of this is in the polynomial estimation.

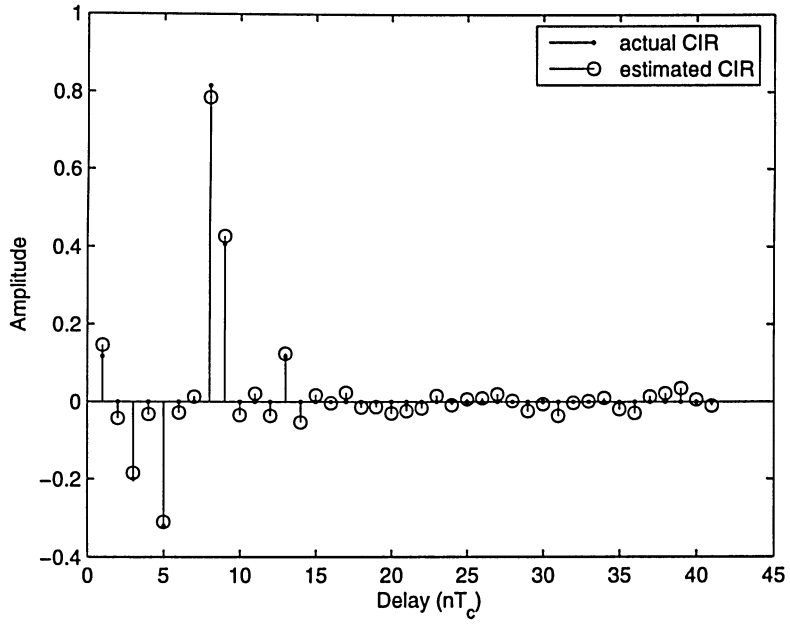

Figure 6.6: 'Good' CIR estimate.

6.2.2 Fiber link identification

Once the CIRs are known, the internal signal $q(n)$ must be estimated so that polynomial fitting can be done between the signals $u(n)$ and $\tilde{q}(n)$. One possible method to estimate the internal signal is by deconvolving $h_{1,\ldots,N}(n)$ with their respective outputs $r_{1,\ldots,N}(n)$. However, estimating the nonlinearity is left for future work since the validity of the CIR estimate can be checked by simply comparing the value of ρ from the downlink to ρ from the uplink. This comparison yields the observation that the 'poor' CIR estimate would give an unacceptable polynomial estimate whereas the 'good' CIR estimate would give an acceptable polynomial estimate. The major contribution here is that the CIRs have been estimated in the presence of a nonlinearity.

6.3 Fiber-wireless downlink equalization

Although the nonlinear channel has not been estimated, equalization can still be performed on the *wireless channel* of the fiber-wireless downlink. The structure of the equalizer is shown in Figure 6.7. The receiver consists only of a linear DFE arrangement that compensates solely

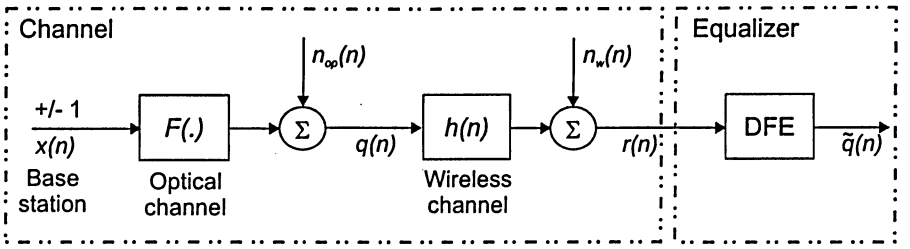

Figure 6.7: Block diagram for fiber-wireless downlink equalization.

for the wireless channel dispersion. Even though the polynomial is not compensated for, the simulation results of the equalization still show a significant improvement in terms of CER. As in the case of the fiber-wireless uplink equalization of Chapter 5, the equalization is done for a single user, but the channel is estimated under a multiuser environment.

Two simulations were performed, one to determine the CER from an 'average' CIR estimate, the other to determine the CER from a 'good' CIR estimate. The DFE parameters were found (as explained in Section 5.3) based on the memory of the CIRs, which were L = 9 ('average') and L = 13 ('good'). The two CER curves are shown in Figure 6.8. The performance of both channels is similar at an SNR < 25 dB, but the 'good' channel outperforms the 'average' channel at higher SNR (> 25 dB). However, a wireless channel is random by nature and so the CIR is dynamic. Therefore, the 'good' channel will not remain good forever and hence a more realistic CER is that of the 'average' channel. Also note that this is the CER, so the BER will be much less. In addition, the error rate can be improved by including a polynomial compensation technique.

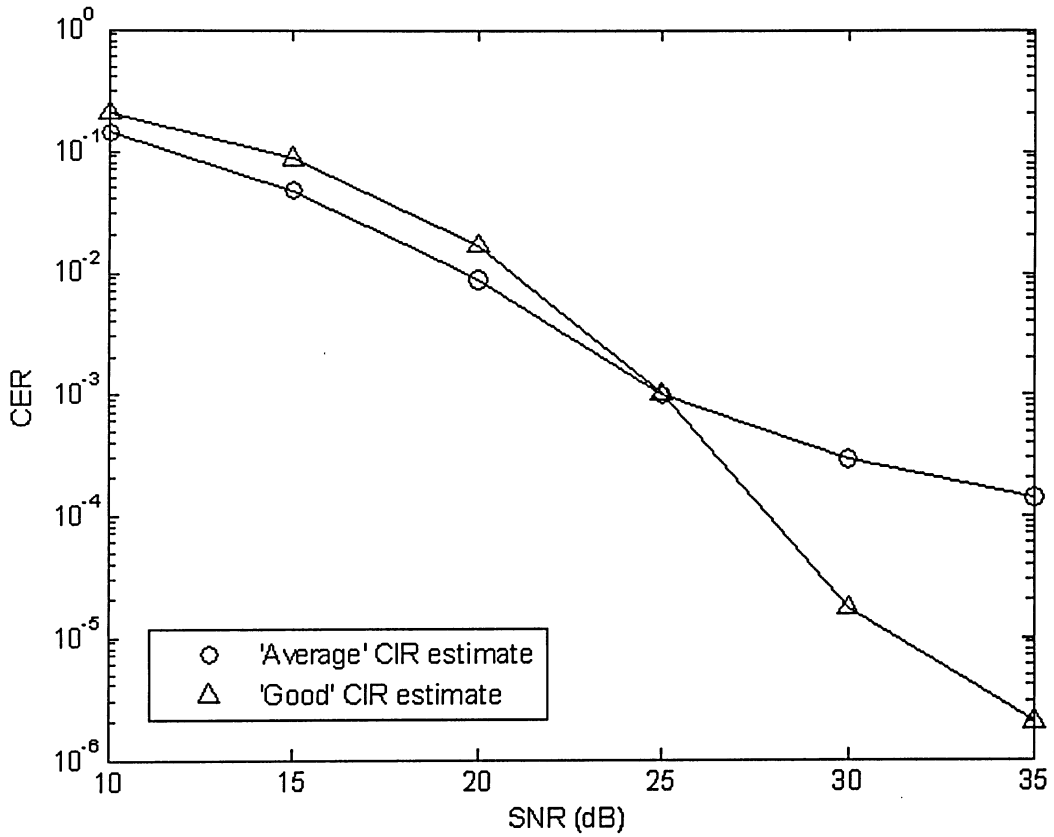

Figure 6.8: CER of fiber-wireless downlink.

Chapter 7

Conclusions and future research

7.1 Conclusions

The projected impact of implementing ROF schemes is substantial. The deployment of optical fiber technology in wireless networks provides great potential for increasing the capacity and quality of service without largely occupying additional radio spectrum. ROF has the potential to become ubiquitous in the communications industry. The research performed in this thesis will bring ROF technology one step closer to providing a cost-effective, high performance solution for present and future high-speed fiber based wireless access systems.

In this study we evaluated two techniques for system identification, one using PN sequences and the other using Walsh codes. We improved the single PN identification performed in [7] to accommodate multiple PN sequences and showed the effect of both wireless and optical channel noise in the output via error rate analysis. Our approach has practical merit in the sense that PN sequences and Walsh codes are already used in existing spread spectrum communication systems. The goal in this thesis was to first estimate the parameters of the fiber-wireless channel and then to devise appropriate equalization and compensation techniques by using these estimates. It was shown that fiber-wireless system identification in a multiuser environment is indeed possible using either PN sequences or Walsh codes, depending on the communication link. Much of the conclusions regarding each fiber-wireless scenario were made in the simulation and discussion sections. The conclusions presented below summarize the observations of the thesis.

The application of nonlinear systems theory to the fiber-wireless uplink (Wiener system)

in a multiuser discrete-time passband system was thoroughly carried out, and an in depth analysis of the correlation relationships in terms of the desired and unwanted terms was discussed. An algorithm to mitigate MAI was developed and shown to significantly improve the estimation in the presence of multiple users. The iterative technique removed most MAI in the system, with a small residual MAI left over. In an asynchronous CDMA environment the proposed identification algorithm works well. The iterative algorithm improved the CIRs quality of fit after just 2 iterations by a significant margin over the initial value. Equalization of the fiber-wireless uplink was done in a single user environment while using the estimated channel parameters from the multiuser case.

Some limitations of the correlation algorithm include:

1. With additional users the identification starts to rapidly degrade.
2. A fairly high SNR is required.
3. The interdependency between the quality of the CIR estimate and the quality of the nonlinear estimate.

Hammerstein system estimation theory was derived for the fiber-wireless downlink in a multiuser discrete-time passband system. It was shown that identification is possible using Walsh codes, but only when multiple Walsh codes are used. The accuracy of the CIR estimation was shown to depend on the CIR characteristics, but overall the algorithm was able to pick out the general structure of the CIR.

7.2 Future research

Although the identification algorithms performed well under certain conditions, there is still a significant amount of research that can be done in order to provide a more realistic and updated simulation model. Suggestions for future work are in the areas of:

Sequence length: The PN sequences and Walsh codes need to be fairly long in order for the identification to work. The reason being the need for good correlation properties. This presents a practical limitation in terms of convergence time and training overhead.

Although sequence lengths have been getting longer, an idea for future work would be to investigate how the correlation properties can be enhanced without the need for longer spreading codes. This would also improve estimation convergence time.

Multilevels: Multilevel testing is required to extract the desired terms in the presence of the nonlinearity. This introduces additional training overhead. Further improvements can be made by investigating how multilevels can be reduced or even eliminated. By doing so, the estimation convergence time would also be improved. Perhaps by recording data while the mobile user is at different locations can provide an alternative to multilevel testing. Another suggestion is to look at higher order input-kernel correlations. This could give additional information about the desired CIR.

Multiuser detection: At this point the channel is estimated in a multiuser environment and then equalized in a single user environment. An idea for future work would be to implement multiuser detection algorithms so that each user is separated from the combined signal and then equalized accordingly. It is important that the selected multiuser detection algorithm work well in a fiber-wireless setting, not just a wireless one.

Complex domain: Instead of estimating the inphase and quadrature phase components of the systems individually, it would be interesting to see the identification procedure evaluated when the theoretical derivation is done in the complex domain.

Estimation approaches: There has been gaining interest in the area of subspace-based system identification. The subspace-based approach is more robust than correlation based techniques and requires modest computational complexity. Implementing the subspace-based approach in a multiuser fiber-wireless CDMA environment has the potential to greatly improve the current technique.

Frequency domain: Shifting analysis from the time domain to the frequency domain is another suggestion. Both the estimation of the fiber-wireless channel as well as analyzing the effects of the nonlinearity can be performed in the frequency domain. The non-

linearity in the ROF system generates distortions of harmonic, intermodulation, and in-band. Analyzing the frequency response of the nonlinear system can provide insight into the systems nonlinear distortions. Different approaches for nonlinear compensation can be validated by checking how close the CER performance with the nonlinear compensator comes to that of the CER in a linear channel.

Fiber-wireless downlink: Only the CIRs were estimated in the fiber-wireless downlink. In order to estimate the nonlinearity, the internal signal must be estimated first. One possible method is by deconvolution.

Appendix A

Multinomial theorem

The multinomial theorem generalizes the expansion of the powers of an expression. It is also a generalization of the binomial theorem. The multinomial theorem is given as

$$(a_1 + a_2 + ... + a_m)^n = \sum_{\substack{n_1,n_2,...,n_m \geq 0 \\ n_1+n_2+...+n_m=n}} C(n; n_1, n_2, ..., n_m) a_1^{n_1} a_2^{n_2} ... a_m^{n_m}, \tag{A.1}$$

where the summation is taken over all indices $(n_1, ..., n_k) \in N$ that satisfy the equation $n_1 + n_2 + ... + n_k = n$, and the multinomial coefficient is given as

$$C(n; n_1, n_2, ..., n_m) = \frac{n!}{n_1! n_2! ... n_m!}. \tag{A.2}$$

For example, with 2 terms and 3$^{\text{rd}}$ order the mutlinomial theorem gives

$$(a_1 + a_2)^3 = a_1^3 + 3a_1^2 a_2 + 3a_1 a_2^2 + a_2^3, \tag{A.3}$$

which is actually the binomial theorem. To see the application of the multinomial theorem to the fiber-wireless channel, consider the single user CDMA output given in equation (4.7), which is repeated here for convenience as

$$r(n) = \sum_{k=1}^{l} A_k \Big(\sum_{m_1=-\infty}^{\infty} ... \sum_{m_k=-\infty}^{\infty} \prod_{i=1}^{k} h(m_i) x(n - m_i) + n_w^k(n) \Big) + \text{ CMT } + n_{op}(n). \tag{A.4}$$

The goal is to determine the quantity defined by CMT above. This can be done using the multinomial theorem. First, some other equations stemming from the single user CDMA environment of Fig. 4.2 are presented. These include the internal signal given by

$$q(n) = h(n) * x(n) + n_w(n) = \sum_{m_1=-\infty}^{\infty} h(m_1) x(n - m_1) + n_w(n), \tag{A.5}$$

and the output given by

$$r(n) = F[q(n)] = A_1 q(n) + A_2 q^2(n) + ... + A_l q^l(n) + n_{op}. \tag{A.6}$$

Let's have a look at the term $A_3 q^3(n)$ in the above equation. Using the multinomial theorem with 2 terms and 3rd order gives the same expansion as that in equation (A.3). Substituting for a_1 and a_2 from equation (A.5) gives the following expression for $A_3 q^3(n)$,

$$A_3 q^3(n) = A_3\Big(\sum_{m_1=-\infty}^{\infty} h(m_1)x(n-m_1) + n_w(n)\Big)^3 \tag{A.7}$$

$$\begin{aligned} &= A_3\Big(\sum_{m_1=-\infty}^{\infty}\sum_{m_2=-\infty}^{\infty}\sum_{m_3=-\infty}^{\infty} h(m_1)h(m_2)h(m_3)x(n-m_1)x(n-m_2)x(n-m_3) \\ &\quad + 3n_w(n)\sum_{m_1=-\infty}^{\infty}\sum_{m_2=-\infty}^{\infty} h(m_1)h(m_2)x(n-m_1)x(n-m_2) \\ &\quad + 3n_w^2(n)\sum_{m_1=-\infty}^{\infty} h(m_1)x(n-m_1) + n_w^3(n)\Big). \end{aligned} \tag{A.8}$$

Therefore, the term CMT in equation (A.4) is given as

$$\begin{aligned} \text{CMT} = A_3\Big(&3n_w(n)\sum_{m_1=-\infty}^{\infty}\sum_{m_2=-\infty}^{\infty} h(m_1)h(m_2)x(n-m_1)x(n-m_2) \\ &+ 3n_w^2(n)\sum_{m_1=-\infty}^{\infty} h(m_1)x(n-m_1)\Big). \end{aligned} \tag{A.9}$$

In the absence of noise, only the term

$$A_3\Big(\sum_{m_1=-\infty}^{\infty}\sum_{m_2=-\infty}^{\infty}\sum_{m_3=-\infty}^{\infty} h(m_1)h(m_2)h(m_3)x(n-m_1)x(n-m_2)x(n-m_3)\Big) \tag{A.10}$$

would be present, but because of the wireless noise there are additional cross multiplied terms which adversely affect the system output, and hence the system identification. The CMT for different numbers of terms and orders can be found following the same procedure.

Bibliography

[1] H. Al-Raweshidy and S. Komaki, *Radio Over Fiber Technologies for Mobile Communications Networks*, 1st ed. Norwood, MA: Artech House Publishers, 2002.

[2] W. I. Way, "Optical Fiber-based Microcellular Systems: An Overview," *IEICE Transactions on Communications*, vol. E76-B, no. 9, pp. 1091–1102, September 1993.

[3] K. Morita and H. Ohtsuka, "The New Generation of Wireless Communications Based on Fiber-Radio Technologies," *IEICE Transactions on Communications*, vol. E76-B, no. 9, pp. 1061–1068, September 1993.

[4] X. N. Fernando, "Signal Processing for Optical Fiber based Wireless Access," Ph.D. dissertation, University of Calgary, 2001.

[5] S. A. Fechtel and H. Meyr, "An Investigation of Channel Estimation and Equalization Techniques for Moderately Rapid Fading HF-Channels," in *Proceedings of the IEEE International Conference on Communications*, vol. 2, June 1991, pp. 768–772.

[6] D. Smalley, "Equalization Concepts: A Tutorial," Texas Instruments," Application report, October 1994.

[7] X. N. Fernando and A. B. Sesay, "Fibre-Wireless Channel Estimation using Correlation Properties of PN Sequences," invited paper, *Canadian Journal of Electrical and Computer Engineering*, vol. 26, no. 2, pp. 43–47, April 2001.

[8] S. A. Billings and S. Y. Fakhouri, "Identification of Nonlinear Systems using Correlation Analysis and Pseudorandom Inputs," *International Journal of Systems Science*, vol. 11, no. 3, pp. 261–279, 1980.

[9] S. Z. Pinter and X. N. Fernando, "Fiber-Wireless Solution for Broadband Multimedia Access," *IEEE Canadian Review*, no. 50, pp. 6–9, Summer 2005.

[10] X. N. Fernando and A. B. Sesay, "Adaptive Asymmetric Linearization of Radio Over Fiber Links for Wireless Access," *IEEE Transactions on Vehicular Technology*, vol. 51, no. 6, pp. 1576–1586, November 2002.

[11] S. A. Billings and S. Y. Fakhouri, "Identification of a Class of Nonlinear Systems using Correlation Analysis," *Proceedings of the IEEE*, vol. 125, no. 7, pp. 691–697, July 1978.

[12] G. Keiser, *Optical Fiber Communications*, 3rd ed. New York, NY: McGraw-Hill, 2000.

[13] P. Raziq and M. Nakagawa, "Semiconductor Laser's Nonlinearity Compensation for DS-CDMA Optical Transmission System by Post Nonlinearity Recovery block," *IEICE Transactions on Communications*, vol. E79-B, no. 3, pp. 424–431, March 1996.

[14] S. Benedetto and E. Biglieri, *Principles of Digital Transmission with Wireless Applications*, 1st ed. New York, NY: Kluwer Academic/Plenum, 1999.

[15] X. N. Fernando and A. B. Sesay, "A Hammerstein type Equalizer for Concatenated Fiber-Wireless Uplink," 2004, to appear in *IEEE Transactions on Vehicular Technology.*

[16] J. C. Gómez and E. Baeyens, "Identification of block-oriented nonlinear systems using orthonormal bases," *Journal of Process Control*, vol. 14, no. 6, pp. 685–697, September 2004.

[17] S. A. Billings and S. Y. Fakhouri, "Identification of Systems Containing Linear Dynamic and Static Nonlinear Elements," *Automatica*, vol. 18, no. 1, pp. 15–26, January 1982.

[18] ——, "Identification of Nonlinear Systems using the Wiener Model," *Electronics Letters*, vol. 13, no. 17, pp. 502–504, August 1977.

[19] M. Schetzen, *The Volterra & Wiener Theories of Nonlinear Systems.* New York, NY: John Wiley & Sons, 1980.

[20] W. J. Rugh, *Nonlinear System Theory – The Volterra/Wiener Approach*, web version ed. Baltimore, MD: The John Hopkins University Press, 1981, Web version prepared in 2002.

[21] M. Schetzen, "Nonlinear System Modeling Based on the Wiener Theory," *Proceedings of the IEEE*, vol. 69, no. 12, pp. 1557–1573, December 1981.

[22] J. G. Proakis, *Digital Communications*, 4th ed. New York, NY: McGraw-Hill, 2001.

[23] B. P. Lathi, *Modern Digital and Analog Communications Systems*, 3rd ed. New York, NY: Oxford University Press, 1998.

[24] Dallas Semiconductor Maxim, "An Introduction to Direct-Sequence Spread-Spectrum Communications," Application note 1890, February 2003.

[25] A. Z. Tirkel, "Cross-Correlation of M-Sequences - Some Unusual Coincidences," in *Proceedings of the IEEE 4th International Symposium on Spread Spectrum Techniques and Applications*, vol. 3, no. 3, 1996, pp. 969–973.

[26] D. V. Sarwate and M. B. Pursley, "Crosscorrelation Properties of Pseudorandom and Related Sequences," *Proceedings of the IEEE*, vol. 68, no. 5, pp. 593–619, May 1980.

[27] R. N. Mutagi, "Pseudo noise sequences for engineers," *Electronics and Communication Engineering Journal*, vol. 8, no. 2, pp. 79–87, April 1996.

[28] B. M. Popovic, "Spreading Sequences for Multicarrier CDMA Systems," *IEEE Transactions on Communications*, vol. 47, no. 6, pp. 918–926, June 1999.

[29] T. Lang and X.-H. Chen, "Comparison of Correlation Parameters of Binary Codes for DS/CDMA Systems," in *Proceedings of the IEEE International Conference on Communications Systems*, vol. 3, November 1994, pp. 1059–1063.

[30] M. Boutayeb and M. Darouach, "Recursive Identification Method for MISO Wiener-Hammerstein Model," *IEEE Transactions on Automatic Control*, vol. 40, no. 2, pp. 287–291, February 1995.

[31] K. S. Narendra and P. G. Gallman, "An Iterative Method for the Identification of Nonlinear Systems using a Hammerstein Model," *IEEE Transactions on Automatic Control*, vol. 11, no. 3, pp. 546–550, July 1966.

[32] M. J. Korenberg and I. W. Hunter, "Two Methods for Identifying Wiener Cascades Having Noninvertible Static Nonlinearities," *Annals of Biomedical Engineering*, vol. 27, no. 6, pp. 793–804, 1999.

[33] Y. Fang and T. W. S. Chow, "Orthogonal Wavelet Neural Networks Applying to Identification of Wiener Model," *IEEE Transactions On Circuits and SystemsI: Fundamental Theory and Applications*, vol. 47, no. 4, pp. 591–593, April 2000.

[34] S. A. Billings and S. Y. Fakhouri, "Non-linear System Identification using the Hammerstein Model," *International Journal of Systems Science*, vol. 10, no. 5, pp. 567–578, May 1979.

[35] E.-W. Bai, "Frequency domain identification of Wiener models," *Automatica*, vol. 39, no. 9, pp. 1521–1530, September 2003.

[36] ——, "Frequency domain identification of Hammerstein models," in *Proceedings of the IEEE Conference on Decision and Control*, vol. 1, December 2002, pp. 1011–1016.

[37] J. C. Gómez and E. Baeyens, "Subspace Identification of Multivariable Hammerstein and Wiener Models," in *Proceedings of the* 15^{th} *IFAC World Congress*, July 2002.

[38] A. A. M. Saleh, "Frequency Independant and Frequency Dependant Nonlinear Models of TWT Amplifiers," *IEEE Transactions on Communications*, vol. COM-29, pp. 1715–1720, November 1981.

[39] K. H. Rosen, *Discrete Mathematics and its Applications*, 4th ed. New York, NY: McGraw-Hill, 1999.

[40] S. Verdú, *Multiuser Detection.* Cambridge, UK: Cambridge University Press, 1998.

[41] P. G. Flikkema, "Spread-Spectrum Techniques for Wireless Communication," *IEEE Signal Processing Magazine*, vol. 14, no. 3, pp. 26–36, May 1997.

[42] X. Fernando and A. Anpalagan, "On the Design of Optical Fiber based Wireless Access Systems," in *Proceedings of the IEEE International Conference on Communications*, vol. 6, June 2004, pp. 3550–3555.

[43] T. S. Rappaport, *Wireless Communications, Principles and Practice.* Upper Saddle River, NJ: Prentice Hall Inc., 1996.

[44] S.-C. Kim, H. L. Bertoni, and M. Stern, "Pulse Propagation Characteristics at 2.4 GHz Inside Buildings," *IEEE Transactions on Vehicular Technology*, vol. 45, no. 3, pp. 579–592, August 1996.

[45] D. P. Taylor, G. M. Vitetta, B. D. Hart, and A. Mammela, "Wireless Channel Equalisation," *European Transactions on Telecommunications*, vol. 9, no. 2, pp. 117–143, March-April 1998.

[46] F. Smyth, A. Kaszubowska, and L. P. Barry, "Overcoming Laser Diode Nonlinearity in Multi-channel Radio-over-fiber Systems," *Optics Communications*, vol. 231, no. 1-6, pp. 217–225, February 2004.

[47] L. Roselli, V. Borgioni, F. Zepparelli, F. Ambrosi, M. Comez, P. Faccin, and A. Casini, "Analog Laser Predistortion for Multiservice Radio-over-fiber Systems," *Journal of Lightwave Technology*, vol. 21, no. 5, pp. 1211–1223, May 2003.

[48] J. Tsimbinos, "Identification and Compensation of Nonlinear Distortion," Ph.D. dissertation, University of South Australia, 1995.

[49] M. Abramowitz and I. A. Stegun, Eds., *Handbook of Mathematical Functions, With Formulas, Graphs, and Mathematical Tables*, 10th ed. Washington, D.C.: U.S. Department of Commerce, 1972.

[50] D. Cypher and S. Wakid, "Error Characteristics of CDMA and Impact on Voice, E-mail, and Web Pages," in *Proceedings of the* 8^{th} *IEEE International Symposium on Personal, Indoor and Mobile Radio Communications*, vol. 2, September 1997, pp. 719–723.

List of publications

Thesis related publications

1. **S. Z. Pinter** and X. N. Fernando, "Estimation and Equalization of Radio-Over-Fiber Uplink in a Multiuser CDMA Environment using PN Spreading Codes," submitted to *IEEE Transactions on Vehicular Technology.*

2. **S. Z. Pinter** and X. N. Fernando, "Equalization of Multiuser Wireless CDMA Downlink Considering Transmitter Nonlinearity using Walsh Codes," submitted to *IEEE Journal on Selected Areas in Communications – Nonlinear Optimization of Communication Systems.*

3. **S. Z. Pinter** and X. N. Fernando, "Fiber-Wireless Solution for Broadband Multimedia Access," *IEEE Canadian Review*, no. 50, pp. 6-9, Summer 2005.

4. X. N. Fernando and **S. Z. Pinter**, "Radio over Fiber for Broadband Wireless Access," *PHOTONS – Technical Review of the Canadian Institute for Photonic Innovations*, vol. 2, no. 1, pp. 24-26, Fall 2004.

5. **S. Z. Pinter** and X. N. Fernando, "Estimation of Radio-Over-Fiber Uplink in a Multiuser CDMA Environment using PN Spreading Codes," in *Proceedings of the IEEE Canadian Conference on Electrical and Computer Engineering*, May 2005, pp. 1-4.

Other publications

1. **S. Z. Pinter** and X. N. Fernando, "Multiwavelength Simulink Model for EDFA Including ASE," submitted to *IEEE Journal of Lightwave Technology.*

2. **S. Pinter**, J. Jiang and X. Fernando, "A Dynamic Multi-Wavelength Simulink Model for EDFA," in *Proceedings of the IEEE Canadian Conference on Electrical and Computer Engineering*, vol. 4, May 2004, pp. 2077-2080.